Complimentary use of dating and hydrochemical tools to assess mixing processes involving centenarian groundwater in a geologically complex alpine karst aquifer

J.M. Gil-Marquez[1], Beatriz De la Torre[1], Matías Mudarra[1], Jürgen Sültenfuß[2], and Bartolomé Andreo Navarro[1]

[1]Universidad de Málaga
[2]University of Bremen

May 5, 2020

Abstract

Environmental dating tracers (^{3}H, ^{3}He, ^{4}He, CFC-12, CFC-11, SF_6) and the natural response of spring (hydrochemistry, water temperature, and hydrodynamics) were jointly used to asses mixing processes and to characterize groundwater flow in a relatively small carbonate aquifer with complex geology in South Spain. Results evidence a marked karst behavior of some temporary outlets, while some perennial springs show buffer and delayed responses to recharge events. There is also a general geochemical evolution pattern, from higher to lower altitudes, in which mineralization and the relation Mg/Ca rises, evidencing longer water-rock interaction. The large SF6 concentrations in groundwater suggest terrigenic production, while CFC-11 values are affected by sorption or degradation. The groundwater age in the perennial springs deduced from CFC-12 and ^{3}H/^{3}He point out to mean residence times of several decades, although the difference between both methods and the large amount of radiogenic 4He in the samples indicates a contribution of old groundwater (free of ^{3}H and CFC-12). Lumped Parameter Models and Shape-Free Models were created based on ^{3}H, tritiogenic ^{3}He, CFC-12, and radiogenic ^{4}He data in order to interpret the age distribution of the samples. The resulting groundwater-age distributions evidence the existence of two mixing components, with an old fraction ranging between 160 and 220 years. Some dating parameters derived from the mixing models and their correlation to physicochemical parameters permits to explain the hydrogeochemical processes occurring within the system. All these results prove that large time residence times are possible in small alpine systems with a clear karst behavior when the geological setting is complex, and they highlight the importance of applying different approaches, including groundwater dating techniques, to completely understand the groundwater flow regime within this type of media.

INTRODUCTION

Environmental tracers are natural or anthropogenic compounds that are widely distributed in the near-surface of the Earth (Cook & Herczeg, 2000; Elliot, 2014). The determination of their concentrations in groundwater allows to estimate its apparent age, which helps on the characterization of the recharge regime of aquifers (Müller et al., 2016; Wilske et al., 2019; Yager et al., 2010), the resolution of mixing process problems (Akesson et al., 2015; Corcho Alvarado et al., 2007), the assessment of groundwater vulnerability to pollution (Jasechko et al., 2017; Musgrove, Solder, Opsahl, & Wilson, 2019), and the development of optimized hydrogeological conceptual models (Gardner & Heilweil, 2014; Sültenfuss, Purtschert, & Führböter, 2011).

Groundwater dating based on environmental tracers, such as radioactive isotopes (^{3}H, ^{14}C,^{36}Cl, ^{85}Kr), noble gases isotopes (^{3}He, ^{4}He, ^{40}Ar), and fluorinated synthetic gases (CFCs, SF_6), has been worldwide used since

the last third of the 20thcentury, particularly in detrital formations (Beyerle et al., 1999; Corcho Alvarado et al., 2007; Mayer et al., 2014; Xu, Gong, & Yang, 2018) and fractured bedrock aquifers (Cook, Solomon, Sanford, Busenberg, & Plummer, 1996; Jaunat et al., 2012; Koh et al., 2018). However, groundwater dating studies based on environmental gas tracers are uncommon in karst hydrogeology, compared to other specific approaches (Goldscheider & Drew, 2007). That is because the interpretation of groundwater ages in karst media is challenging due to the high heterogeneity commonly found in these aquifers. While groundwater flows rapidly through conduits and fractures, the flow velocity in the matrix or small fissures is very slow (Han, Hacker, & Gröning, 2007; Worthington & Gunn, 2009). Such characteristics would require the joint application of several environmental tracers that help to constrain the age distribution of groundwater (Wilske et al., 2019), particularly if a comprehensive understanding of groundwater flow behavior is not achieved based on other experimental methodologies (hydrodynamic, hydrothermal, hydrochemical, and stable isotopes).

During the last couple of decades, several studies have demonstrated the applicability of environmental tracers for groundwater dating in karst systems, which allow to better understand flow dynamics. In general terms, they found a mixing between recently infiltrated water and older groundwater components. The old fraction in the mix may have a few decades (Delbart et al., 2014; Jiang, Guo, & Tang, 2019) or, more commonly, was infiltrated before the middle of the 20th Century, previously to the anthropogenic release of ^{3}H and CFCs (Han et al., 2007; Long & Putnam, 2009; Toth & Katz, 2006; Yager et al., 2010; Zang, Zheng, Qin, & Jia, 2015). In regional carbonate aquifers, some of which are partially confined, the dating of the old groundwater components often indicates ages of hundreds or even thousands of years (Land & Huff, 2010; Müller et al., 2016; Musgrove et al., 2019; Plummer, Busby, Lee, & Hanshaw, 1990; Xanke et al., 2015). However, karst aquifers in alpine mountains are generally characterized by recently infiltrated young groundwater, with maximum mean recharge dates of a few years, although sometimes mixed with a low percentage of older components (Althaus et al., 2009; Rank, Volkl, Maloszewski, & Stichler, 1992; Shah, Jeelani, & Jacob, 2017).

Alpine karst occupies areas of high altitude and is characterized by pronounced relief, commonly intense tectonic deformation deriving in a strong hydrogeological complexity, and sparse or absent vegetal and soil covers (Field, 1999; Palmer, 1984). The large height variations existing in alpine karst generally imply a thick unsaturated zone and high hydraulic gradients, resulting in rapid flow velocities and short residence times within the conduit network (Werner, 1979). All these characteristics are enhanced in small aquifers. Though alpine karst formations are named after the Alps (Central Europe), this type of karst is worldwide extended, particularly in Europe (Ballesteros, Jiménez-Sánchez, Giralt, García-Sansegundo, & Meléndez-Asensio, 2015; Lauber & Goldscheider, 2014; Mudarra & Andreo, 2011; Turk et al., 2015), Asia (Ebrahimi, Pasandi, & Ahmadipour, 2007; Shah et al., 2017; Wu et al., 2019), and North America (Ford, 1983; Smart, 1988; Spangler, 2001).

The main goal of this work is to highlight the complementarity of conventional hydrogeological tools and groundwater dating techniques as an effective approach to evaluate mixing processes involving components of different ages in geologically complex karst areas located in alpine mountains. To do so, environmental dating tracer data (^{3}H, $^{3}He_{trit}$,$^{4}He_{rad}$, CFC-12, CFC-11, and SF_6) and the hydrodynamic, hydrochemical, and groundwater temperature data series from several springs draining a relatively small and complex alpine karst aquifer (Jarastepar) in South Spain are jointly considered. Based on the concentration of environmental dating tracers in the samples, Lumped Parameter Models, and Shape-Free Models were created to assess the groundwater age distribution in diverse water conditions. The simultaneous application of different methodologies provides a significant and quantitative advance in the hydrogeological knowledge of the karst system, from which an improved conceptual model of the aquifer functioning can be established (basis for numerical model), more solid than if convetional hydrogeological tools or dating techniques would have been individually applied. This joint approach is uncommon in alpine karst hydrogeology, but it can be useful in particular cases in which conventional hydrogeological methods do not explain the whole complexity of the aquifer.

SETTING

The pilot site is located in the central part of the Ronda Mountains, in southern Spain (Fig. 1). The catchment area covers a rugged land surface of 56 km^2 (38 km^2 of carbonate rocks) with altitudes ranging from 400 to 1400 m a.s.l. and an average slope of 20 %. The climate is Mediterranean type. The mean precipitaiton in the area is 1,050 mm/yr, and rainfall generally occurs between autumn and springtime. The averages values of precipitation and temperature recorded at the Jarastepar meteorological station (1,317 m a.s.l.; Fig. 1) during the research period (October 2014 to December 2016) are 770 mm/yr and 12.2 ºC, respectively. However, during the recharge times, an average temperature of 8 ºC was recorded.

From a geological standpoint, the research area presents a complex structure that involves rocks from three main tectonic domains of the Betic Cordillera (Figs. 1 & 2): a) the External Zone (EZ) occupying the lowest tectonic position and lithostratigraphically formed, from the bottom to the top, by Upper Triassic clays and evaporites, Jurassic dolostones and limestones (>500 m thick), and Cretaceous-Tertiary marly-limestones and marls (Martín-Algarra, 1987); b) the Internal Zone (IZ), overlapping the External Zone from the southwest, composed of up 400 m of Paleozoic metamorphic rocks (mainly schists) and more than 1,000 m of carbonate formations (mainly dolostones); c) Flysch Complex (FC), formed by Tertiary clays and sandstones and discontinuously imbricated between the two previous domains (defining the tectonic suture). The geological structure of the EZ is characterized by a NE-SW anticlinorium fold, which overthrusts with vergence toward the NW over the Triassic clays of the anticline core. Likewise, the internal structure of carbonate formations from the IZ corresponds to the normal limb of a large ENE-WSW-trending north-verging synform developed eastward of the study area (Martín-Algarra, 1987). The set of geological units were affected by more recent strike-slip faults (NW-SE) and normal fractures (NE-SW and N-S) (Fig. 1).

In hydrogeological terms, the Jarastepar aquifer is comprised of fractured and karstified Triassic (IZ) and Jurassic (EZ) carbonate rocks that are bounded by low permeability formations, mainly Triassic clays and Cretaceous-Paleogene marls of the EZ (Fig 1). However, the southern border coincides with a major tectonic contact between the materials of the EZ and the IZ, involving rocks with very different permeabilities (Fig. 2). Recharge occurs by rainfall infiltration over the carbonate outcrops (predominantly diffuse but locally concentrated through swallow holes), while discharge takes place through springs located in the southern border of the aquifer. There are three perennial outlets (Huertos -560 m a.s.l.-, Charco -589 m a.s.l.- and La Zúa -603 m a.s.l.-) that are located in the tectonic contact between the Triassic dolostones and the metamorphic rocks of the IZ. There is also a temporary discharge area (overflow springs -643 - 664 m a.s.l.-) at the southern edge of the EZ, just North of the major tectonic contact (where low permeable Flysch clays are imbricated) between the IZ and the EZ. In low water conditions, the water table is accessible through a shaft with a vertical development of 40 m in the overflow point.

METHODS

From October 2014 to December 2016 water temperature and electrical conductivity (EC) were hourly recorded in La Zúa (WTW^{TM} Cond 315i), Charco, and Huertos springs (HOBO^{TM} Onset U24-001), as well as in the shaft of the overflow springs (OTT EcoLog-800). The water level variations were registered in La Zua (Odyssey^{TM} Capacitance Water Level) and the shaft (OTT EcoLog-800) and later transformed to flow-rate data series. Additionally, single flow measurements were made in all the outlets and samples for hydrochemical analysis were collected, with a weekly to daily periodicity (depending on the hydroclimatic conditions).

Samples for major ion chemistry analysis were taken in 125 ml amber glass bottles, while 1L PET bottles were used for ^{3}H analysis. For noble gas determination, spring water was conducted through a transparent tube and collected into duplicate clamped-off copper cylinders, using a 12v submersible pump, following the procedure described by Sultenfuss *et al.* (2011). For CFC and SF_6 analysis, samples were collected in 500 ml double-opening steel bottles, as explained by Jaunat *et al.*(2012). To avoid modern-air contamination, a Viton hose was used to bring the water from the spring to the bottles. Suction was created using a peristaltic pump with a transparent tubing-outlet, which permitted the detection of bubbles that would

indicate induced degassing. The steel bottles were shaken after sealing, so the lack of noise permitted to discard the involuntary formation of a headspace. Samples for groundwater dating were collected on five different dates, coinciding with diverse hydrodynamic situations: low, intermediate and high water conditions (LW, IW, and HW in Fig. 3).

Major chemical components were determined in the Laboratory of the Centre of Hydrogeology of the University of Malaga (CEHIUMA). Alkalinity was analyzed by volumetric titration with 0.02N H_2SO_4 to pH 4.45. Major ions (Ca^{2+}, Mg^{2+}, Na^{+}, K^{+}, Cl^{-}, SO_4^{2-}) were determined by ionic chromatography (METROHM Compact 930 IC flex for cations and Compact 881 IC Pro for anions). Determination of ^{3}H, He isotopes, Ne, CFC, and SF_6 was carried out in the Department of Oceanography of the Institute of Environmental Physics, University of Bremen. He isotopes, Ne, and ^{3}H were determined in the mass spectrometric facility described by Sultenfuss, Roether, and Rhein (2009). The ^{3}H analysis followed the^{3}He–ingrowth method (Clarke, Jenkins, & Top, 1976), so water samples of 0.5 kg were degassed and stored in gas-free glass bulbs for production and accumulation of ^{3}He, the decay product of ^{3}H. After 4-6 months of storing, the produced ^{3}He was determined with the mass spectrometric system. On the other hand, CFC and SF_6concentrations were determined using a micro electron capture detector (micro-ECD) mounted on a gas chromatograph (Agilent GC6890N) with a capillary column, as explained by Bulsiewicz, Rose, Klatt, Putzka, and Roether (1998). The CFC data were calibrated according to the SIO scale 2005 (Bullister & Tanhua, 2010).

Noble gas concentrations are expressed in ccSTP/kg of H_2O and the specific radioactive activity of^{3}H is referred to Tritium Units (TU = 0.119 Bq/kg of H_2O). The CFC and SF_6 concentrations (pmol/kg of H_2O) were converted to atmospheric mixing ratio (pptv) according to the recharge conditions: average recharge altitude of 1,150 m a.s.l., mean temperature of 8 oC during rainy months (October to May), and no salinity. The potential contribution of excess air was quantified as proposed by Aeschbach-Hertig, Peeters, Beyerle, and Kipfer (1999), based on the mean ΔNe values of each sample point. ΔNe is the difference between the concentrations of Ne in the sample and its theoretical content at recharge conditions minus 1, expressed in percentage.

Groundwater age of the sample fraction containing ^{3}H (recharged after 1953), was calculated by the^{3}H/^{3}He method (Torgersen, Clarke, & Jenkins, 1978). The apparent piston flow^{3}H/^{3}He age (τ) is given by:

$$\tau = \frac{1}{\lambda} ln\left(1 + \frac{^3He_{trit}}{^3He}\right) \text{(Equation 1)}$$

where λ is the ^{3}H decay constant, of 0.05626 yr^{-1} (ln(2)/12.32 yr; Lucas and Unterweger, 2000), and^3He_{trit} (tritiogenic^{3}He) is the concentration of that isotope in the sample derived from ^{3}H decay. Its separation from other ^{3}He sources in groundwater (equilibrium, excess-air, radiogenic) is possible using ^{4}He and Ne data (e.g. Cook & Herczeg, 2000; Sültenfuss et al., 2011). The CFC and SF_6 ages were determined by comparing their concentration in the sample and their mixing ratio in the Northern Hemisphere atmosphere (USGS, 2018). The ^{3}H input function used in modeling tasks was generated from the correlation of the ^{3}H in precipitation recorded by the GNIP (Global Network of Isotopes in Precipitation) station closest to the pilot site (Morón, 55km northwards) and the data series of the GNIP Vienna station (IAEA/WMO, 2018). The resulting function was scaled to 2016; that is, it was converted to current concentration using the radioactive decay law and the ^{3}H decay constant. The difference from the original and the decayed ^{3}H input functions give rise to a ^{3}He_{trit} input function.

To interpret the groundwater age distributions of each sample, different models were created based on the concentration of ^{3}H,^{3}He_{trit},^{4}He_{rad} (radiogenic^{4}He) and CFC-12 in samples taken during the same hydrodynamic conditions: high water or intermediates water (Tab. 2). The software TracerLPM (Jurgens, Böhlke, Eberts, & Survey, 2012) was used for developing Lumped Parameter Models -LPMs- (Maloszewski & Zuber, 1982). This kind of model uses a convolution integral to sum up all the tracer concentrations (C_i) at each possible time (t '). It incorporates a weight function *g(t-t')*determining the importance of each age in the total groundwater age at the sampling time (t) and a decay term for radioactive tracers based on the decay constant (λ):

$C_s(t) = \int_{-\infty}^{t} C_i(t')g(t-t')e^{-\lambda\left(t-t'\right)}dt'$(Equation 2)

Additionally, Shape-Free models were created (Visser, Broers, Purtschert, Sültenfuß, & de Jonge, 2013). This approach is a simplification of equation 2, but instead of using a weight function, it describes the groundwater age distribution of the sample as a histogram of n bins, each of which has a uniform age. The number of bins is constrained by the number of tracers considered (n - *1*). The measured tracer concentration in the sample (C_s) is the result of summing the products of the mean tracer concentration in each bin (C_i) and the fraction they represent in the whole groundwater sample (F_i):

$C_s(t) = \sum_{i=1}^{n} F_i C_i(t')$ (Equation 3)

Two Shape-Free Models (SFMs) were used to describe the groundwater age distribution of each sample: 5-bin models were created based on the four more reliable tracers (CFC-12, ^{3}H,^{3}He$_{\mathrm{trit}}$, and^{4}He$_{\mathrm{rad}}$) and 4-bin models were derived from the three young groundwater tracers. The latter model does not include ^{4}He data because its accumulation rate is uncertain. In both cases, all the bins are equidistant except for the oldest one, which represents a sample fraction without recent age tracers (i.e., ^{3}H,^{3}He$_{\mathrm{trit}}$, and CFC). The characteristics of each bin are shown in table 3. The SFMs were developed using SOLVER Add-In in Excel. Each bin fraction was calculated adopting as constrains the piston-flow concentrations of the selected tracers in the sample.

RESULTS

Hydrodynamics and hydrochemistry

During the research period, the mean flow rates of the perennial outlets (IZ) varied from 23.4 l/s (Charco spring) to 208 l/s (La Zúa spring), with coefficients of variation comprised between 15.1% and 16.1%, respectively (Tab. 1). These springs show buffered and delayed hydrodynamic responses to recharge events, reaching the flow peaks in several weeks or even months (Fig. 3). On the contrary, the discharge rate in the overflow area during activity periods has an average value of 2.3 m^3/s, though it can reach 21.4 m^3/s. The water level variations in the shaft of the overflow area denote a marked karst behavior, with quick rises as a response to rainfall, as well as rapid falls (Fig. 3).

The mean contents of Ca^{2+}, Mg^{2+}, and SO_4^{2-} in the overflow springs are respectively 65.4 mg/l, 5.1 mg/l, and 8.3 mg/l, while alkalinity is 203.5 mg/l (Tab. 1). The mineralization of groundwater greatly increases towards lower altitudes in the IZ (Fig. 3), particularly Ca^{2+}, Mg^{2+}, and SO_4^{2-}, which respectively reach average values up to 437.3 mg/l, 87 mg/l, and 1201.1 mg/l in Huertos spring (Tab. 1). These changes in the hydrochemistry of groundwater cause the rise of EC toward lower altitudes (Fig. 3), from mean values of 352 µS/cm in the overflow outlets, to averages comprised between 1565 µS/cm and 1875 µS/cm in the IZ (Tab. 1). Likewise, the mean temperature value of the groundwater drained through the overflow area is 14.9 ºC, while it is comprised between 15.7 ºC and 16.7 ºC in the IZ springs.

The variability of the physicochemical parameters monitored in the overflow springs is much higher than in the outlets of the IZ, as it is shown by their coefficients of variation (Tab. 1). While the water temperature and the EC values registered in the overflow area change greatly and rapidly, the variations of these two parameters are smoother and delayed in the perennial springs of the IZ. It is also observed that the concentration of Mg^{2+} is more stable than the contents of Ca^{2+} and SO_4^{2-} (Fig. 3). However, Mg^{2+} and SO_4^{2-} are more stable in the overflow area than in the perennial outlets (Fig. 3). Hence, the temporal hydrochemical evolution of the springs reflects two clear distinct patterns depending on the geological location of the springs in the aquifer (Fig. 3).

Environmental tracers

The ΔNe values of the samples are comprised between 27.0% and 39.4%, showing certain air excess in the samples (Tab. 2). The ΔNe of the duplicate differs 5% at most, so the excess is not due to an inadequate sampling process, but rather to the dissolution of air bubbles that are trapped in the soil zone or the aquifer during recharge (Aeschbach-Hertig et al., 1999; Mayer et al., 2014). The ΔNe values permit to estimate

the fraction of gases in the sample coming from excess air, including ^{4}He isotopes (Aeschbach-Hertig et al., 1999). Non-atmospheric ^{4}He is of underground radiogenic origin ($^4He_{rad}$) and produced by alpha decay of the U and Th decay series. The rest^{4}He comes from the atmosphere (solubility equilibrium). Assuming that the liberation rate of the$^4He_{rad}$ to groundwater is constant and homogeneous, its concentration would be proportional to groundwater travel time (Solomon, 2000). The concentrations of$^4He_{rad}$ in the samples range from $1.3 \cdot 10^{-5}$ to $2.6 \cdot 10^{-5}$ ccSTP/kg (Tab. 2). A rise in the content of $^4He_{rad}$ is observed from La Zúa to Huertos spring, from higher to lower altitudes (Fig. 4), which would indicate also an increase of the mean residence time. The $^4He_{rad}$ accumulation rates reported in the literature vary two order of magnitude, from $2.0 \cdot 10^{-8}$STPcc·kg^{-1}·yr^{-1} (Lehmann et al., 2003) to $1.9 \cdot 10^{-6}$STPcc·kg^{-1}·yr^{-1} (Beyerle et al., 1999), so it is not possible to estimate a reliable$^4He_{rad}$ age using these values. Nevertheless, assuming the fastest accumulation rate, of $1.9 \cdot 10^{-6}$STPcc·kg^{-1}·yr^{-1}, the observed data would require at least transit time of nearly a decade, although slowest accumulation rates would lead to transit times up to two orders of magnitude higher.

All the samples contain ^{3}H, between 1.65 and 2.46 TU (Tab. 2). The ^{3}H activity in precipitation registered in SW Spain by the GNIP from 1980 (IAEA/WMO, 2018) scaled to 2016 is in the same range (De la Torre, 2020). Therefore, the concentrations observed in the samples could correspond to piston flow ages within that period; in other words, an unmixed groundwater sample with that^{3}H content would have been recharged within that interval. The ^{3}H/^{3}He dating results show infiltration ages between 33 and 40 years (Tab. 2), which could be fairly consistent with the mentioned period. However, small rises in the^{3}H/^{3}He ages (2 years) would be related to ^{3}H activities that duplicate the observed data. Therefore, mixing with a tritium-free component cannot be completely discarded.

The measured CFC-12 values vary from 0.98 and 1.58 pmol/kg, which correspond to atmospheric mixing ratios of 184 and 295 pptv (Tab. 2) at the infiltration conditions of temperature and pressure. Note that the effect of using different ΔNe within the observed range in each spring would affect the CFC-12 mixing ratios in less than 5 pptv, which do not have a practical effect on dating estimations. The results would indicate piston flow ages from 36 to 43 years, which are slightly older than the ^{3}H/^{3}He ages (Tab. 2). Such differences could be related to the dilution of the CFC-12 concentration due to the presence of an old component with a lower tracer content or free of it. That dilution would produce a bias towards older CFC-12 ages, but it would not modify the^{3}H/^{3}He. A CFC-12 diminishing could be also produced by sorption or microbial degradation, although it seems unlikely in this case since CFC-12 sorption is generally negligible (Cook & Solomon, 1997) and its degradation requires anoxic conditions (IAEA, 2006), which is not the case in the springs of the IZ (mean dissolve oxygen = 4.5 mg/l).

CFC-11 values are comprised between 1.27 and 2.28 pmol/kg, equivalent to 62 and 111 pptv, respectively (Tab. 2). Such values are much lower than the expected from the CFC-12 data and are not explainable by applying mixing models. As no contamination sources exist in the recharge area, the CFC-11 concentrations in groundwater have to be diminished by sorption or another physical or biochemical process (IAEA, 2006). On the contrary, the contents of SF_6 in the sample (0.17 - 0.22 pmol/kg) are related to extremely high SF_6 mixing ratios, over 450 pptv (Tab. 2). Such results are more than one order of magnitude higher than the current atmospheric mixing ratios (approximately 10 pptv) and without a near pollution source, they can be explained only by a terrigenic production. The dominance of dolostone formations in the aquifer may be the natural source of SF_6 (Busenberg and Plummer, 2000). Neither the CFC-11 nor the SF_6 are reliable to be included in the mixing models.

Groundwater mixing and age distribution models

To find a model that properly describes the groundwater age distribution of the samples, each possible type of Lumped Parameter Models (LPMs) was checked: Piston Flow Model –PFM-, Exponential Model –EM-, Partial Exponential Model –PEM-, Exponential Piston Model –EPM- and Dispersion Model –DM- (e.g. Jurgens et al., 2012; Suckow, 2014). In general terms, none of them show a good fitting to the sample concentrations. However, according to the PFM and the DM (dispersion parameter = 0.05), a binary mixing process could explain the tracer concentrations. In Figure 5, the spring samples are plotted in three tracer-tracer graphs together with the evolution of the tracers. The samples plot in areas between two theoretical

mixing lines drawn from an old component (200 years) to two different modern groundwater components, of 0 and 40 years (Fig. 5). This suggests that the tracer concentration measured in the sample could be explained by a Binary Mixing Model (BMM). Based on that, two BMMs were created for each sample, one of them combines two PFM as a simplified proxy, and the other one integer two DM, which is a type of LPM that does not need previous assumptions about the flow conditions. The dispersion parameter of the DM that describes the young fraction of the DMM is 0.05, and its mean age range from 25 to 31 years, depending on the sample. The dispersion parameter in the old DM is 0.2, and the mean ages are 160 years for La Zúa spring, 180 years for Charco spring, and 220 years for Huertos spring.

Different accumulation rates of $^4He_{rad}$were checked to include it in the LPMs. The best results were found using a value of $2{\cdot}10^{-7}$STPcc$\cdot$kg$^{-1}\cdot$yr^{-1}. This rate permitted estimate an apparent $^4He_{rad}$ age for each sample (Tab. 2) that varies between 66 years (La Zúa) and 131 years (Charco). These values are not the same as the ones used to define the old fraction of the LPM, as the $^4He_{rad}$content in the sample would be diluted by the younger component. The$^4He_{rad}$ accumulation rate has permitted to include this tracer to create a SFM of 5 bins. As the concentration of this tracer in each bin is estimated from another model (BMM DM-DM), the 4-bin SFM has been also generated without$^4He_{rad}$.

In Table 4 there is a summary of the main information extracted from each of the models. Both types of LPMs suggest that the percentage of the old component (free of ^{3}H and CFC-12) is greater in Huertos spring, while its ratio is lower in La Zúa. This pattern is also observed in the results obtained from the application of SFMs (Tab. 4). Therefore, the proportion of groundwater infiltrated before 1940 increases towards lower altitudes.

The mean age of the groundwater samples only could be estimated by those models that include the $^4He_{rad}$ data (BMM DM-DM and 5-bin SFM), as the other two models (BMM PFM-PFM and 4-bin SFM) were created based only on ^{3}H and CFC-12 that do not provide information about the age of the old fraction of the samples. The mean age results of each sample differ considerably depending on the model (Tab. 4), from 15 years of difference in La Zúa spring (54 and 69 years) to 35 years in Huertos spring (95 and 123 years). Nonetheless, in both cases, the mean age of the samples increases from the highest altitude (La Zúa) to the lowest height (Huertos). It is also noteworthy that all the mean ages indicate several decades of average transit time. Ages older than 63 years would indicate a mean infiltration date before the anthropogenic liberation of^{3}H (1953), while values higher than 76 would also be previous to the generation of CFC-12 (1940).

The groundwater age distribution of the samples was calculated by applying the LPMs and the SFMs (Fig. 6). All the models show that La Zúa spring accumulates sooner a higher proportion of young water, while the groundwater age distributions of the samples from Charco and Huertos springs are progressively biased towards older ages. The two samples of Huertos and Charco springs show similar distribution, independently on the hydrodynamic conditions in which they were collected, while the samples of La Zúa springs show some differences (Fig. 6); the sample taken in high water conditions (December 2016) accumulates less proportion of young groundwater than the one collected in an intermediate water state (October 2014).

The median of the Groundwater Age distribution (hereby GA50) can be easily identified in groundwater distribution plots, in that bin (for SFM) or age (for LPM) in which the cumulative fraction reaches or exceeds the 50% (Gil-Márquez, Sültenfuß, Andreo, & Mudarra, 2020). This parameter permits to rapidly assess whether the sample is mainly formed by recent or older groundwater, contrary to the mean age, which sometimes leads to misinterpretation of mixed groundwater age data. The GA_{50} could reach more than 80 years in all the spring according to the 5-bin SFM (Tab. 4 and Fig. 6), while the lowest values are obtained from the BMM DM-DM, with GA_{50} of 30 years in La Zúa spring, 44 years in Charco, and 60 years in Huertos. Thus, the groundwater drained by the spring accumulates less modern fraction towards lower altitudes.

DISCUSSION

Coupling hydrochemistry and groundwater age distribution

The variations of the dating environmental-tracer concentrations under different hydrodynamic conditions (Tab. 2) permit obtaining information about the functioning of the aquifer. Particularly, it is observed that the $^4He_{rad}$ concentration rises from high water (HW) to low water (LW) conditions. It would indicate that during recession periods the mix of groundwater drained through the spring is older than in discharge rises. That is in agreement with the registered increment of mineralization in the dry periods (Fig. 3). The only exception to the pattern is found in La Zúa spring, where the highest $^4He_{rad}$ content was measured in high water conditions (Tab. 2). That can be explained because during the sampling the spring was showing a piston-flow effect (Fig. 3). This term is used in karst hydrogeology to indicate a rise of mineralization and water temperature in the spring as a response to recharge events, which is often produced by mobilization of older groundwater from the saturated zone (Mudarra & Andreo, 2011). The decrease of^{3}H concentration in low water conditions (Tab. 2) could also be produced by a higher proportion of old groundwater (tritium-free) being drained. However, the evolution of the^{3}H input function and the seasonal fluctuation of the activity of this isotope in the atmosphere make it difficult to obtained further conclusions with only a few samples. Delbart et al. (2014) proved that a more exhaustive sampling routine would help to understand the evolution of young-groundwater tracer (not only ^{3}H but also CFC and SF_6), particularly during discharge rises. In that sense, the present work also demonstrates the potentiality of an old-groundwater tracer ($^4He_{rad}$) to analyze the natural response of karst springs.

In Figure 7, some physicochemical and chemical parameters are compared to groundwater dating data derived from the LPMs and the SFMs. It is observed that electrical conductivity (EC) is positively related to the proportion of old groundwater (free of ^{3}H and CFC-12) and the mean and median age of the samples (Fig. 7A & B). The ascent of EC is also related to a decrease in the spring height (Fig. 3). That combined indicates that the groundwater drained by the springs located at lower altitudes would have longer residence time within the aquifer, thus it would have dissolved a greater amount of solutes (i.e., higher EC).

A similar relationship is established between the groundwater dating parameters and the temperature values measured in the spring water (Fig. 7C & D), which are slightly higher (1-2^{o}C) than the mean annual temperature of the area (De la Torre, Mudarra, & Andreo, 2020). Besides, the variability of the water temperature of the springs located in the IZ is low (<1%), contrary to the variability of the flow rate and most of the chemical parameters (Tab. 1), and also to the groundwater temperature in the overflow area. All this information suggests that groundwater may flow within deep areas of the system. However, the lack of thermalism *stricto sensu* would indicate a slow ascent of groundwater flows toward the discharge points, reaching progressively temperature values near the equilibrium with the atmospheric ones.

The water mineralization of the springs placed in the IZ is mainly related to dissolved SO_4^{2-}, Ca^{2+}, and Mg^{2+} contents (Tab. 1). The presence of SO_4^{2-} and Ca^{2+} in the groundwater of Jarastepar aquifer allows the dedolomitization of the Triassic dolostone rocks belonging to the EZ. This geochemical process involves multi-mineral phases and consists in the transformation of dolomite crystals in calcite (Appelo & Postma, 2005; Wigley, 1973), resulting in a greater amount of dissolved Mg^{2+} in groundwater than that explained by dolomite dissolution only. While the concentration of Mg^{2+} in groundwater shows a marked increase towards lower altitudes, the rise of Ca^{2+} is less steep (Fig. 3). Besides, the molar relation between Mg^{2+} and Ca^{2+}(rMg/Ca) presents a positive and well-defined relationship with the percentage of old groundwater in the samples and their mean and median ages (Fig. 7E & F). Therefore, there is an enrichment of Mg^{2+} respect to Ca^{2+} as groundwater became older. That indicates that the groundwater drained at lower altitudes is hidrogeochemically more evolved due to longer water-rock interactions. This process has been also are described in other carbonate systems worlwide (Carucci, Petitta, & Aravena, 2012; McMahon, Bohlke, & Christenson, 2004; Moral, Cruz-Sanjulian, & Olias, 2008; Plummer et al., 1990). Besides, the good correlation degree between the dating parameters obtained from the models and the rMg/Ca indicates that the groundwater of Jarastepar aquifer is mainly stored in dolomite-bearing formations, which form the permeable layers in the IZ and the deepest part of the aquifer in the EZ (Figs. 1 & 2).

The dissolution of the evaporite rocks from the EZ is the main source of SO_4^{2-} and Ca^{2+} in the groundwater of the aquifer, according to the high stoichiometric relation of both ions and to the isotope signature of

$\delta^{34}S_{SO4}$ and $\delta^{18}O_{SO4}$ (De la Torre et al., 2020). The SO_4^{2-} concentration in the samples is positively related to the presence of old groundwater and the mean and median ages (Fig. 7G & H). However, the correlation degrees are lower than those found for EC and rMg/Ca. That could indicate that gypsum dissolution does not occur during all the groundwater transit time, contrary to dedolomitization. Thus, groundwater would dissolve gypsum within the EZ substratum, which would enhance the gaining of Mg^{2+} through dedolomitization, although it cannot be discarded that some of the Mg^{2+} present in the groundwater would come from the dissolution of evaporite rocks (Hamill & Bell, 1986; Chenini, Farhat & Ben Mammou, 2010.). After groundwater enters the IZ, the dissolution of gypsum ends (since there are no evaporites in the IZ), but the SO_4^{2-}concentration is still high, allowing dedolomitization to last longer while groundwater flows within the Triassic dolostone formation.

The low correlation degree between the groundwater age parameters and SO_4^{2-} is somewhat produced by the large variations of the concentration of this ion in the spring waters, particularly in La Zúa (Fig. 7G & H). The higher outflow rate in La Zúa spring and its greater hydrodynamic response (Tab. 1, Fig. 3) denotes a better hydrogeological connection with the External Zone. That would explain the higher variability of SO_4^{2-}, but also the changes in the groundwater age distribution that are observed in every model made from the samples of the spring (Tab. 4; Fig. 7). Despite the groundwater age distribution of Huertos and Charco springs do not evidence many variations, it cannot be discarded that a higher number of analyses of dating environmental tracers could show otherwise.

Implications of the geological setting on the groundwater residence time

All the SFMs show significant accumulation of groundwater between the 20 and 60 first years, while the fraction does not change in the immediately following bin (Fig. 6). Therefore, the remaining groundwater fraction is attributable to the old bin (free of ^3H and CFC-12). The groundwater age distributions obtained from the SFMs, which do not require any previous assumption of the hydrogeological functioning of the system, agree with the binary mixing LPMs that were proposed. Thus, they confirm that the drainage of Jarastepar aquifer is explained by two main flow components. One is formed by groundwater age infiltrated during the last few decades, while the other one has a greater mean residence time of around 200 years. The groundwater age distribution of the springs of the IZ contrast with the high flow velocities determined in the EZ of the aquifer (overflow area in figure 1) using dye tracing tests, which reached 600 m/h (De la Torre, 2020).

The rocks of the EZ have a large development of the conduit network, with a great drainage capacity that allows the fast arrival of recently infiltrated water towards the overflow area. There, temporary outlets drain the aquifer only when the water coming from recharge exceeds the transfer capacity between the IZ and the EZ, due to the hydarulica hetereogeneity of the media. The chemical signature of the groundwater drained through the overflow area and the dye tracing experiences evidence that the origin of the groundwater drained through this area is mostly related to the recharge events that give rise to the activation of the temporary outlets, and it has a mean residence time of 54-64 hours (De la Torre et al., 2020). This behavior is typical in karst areas, where the mean residence time of groundwater is between tens of hours to several months, inferred by using natural and artificial responses of the springs (Barbera et al., 2018; Birk, Liedl, & Sauter, 2004; Lauber & Goldscheider, 2014; Perrin, Jeannin, & Zwahlen, 2003; Shah et al., 2017). However, those age estimation only reflect the fastest flowpaths throughout the conducts but not the slower flows through narrow fractures and the matrix, which must be estimated based on environmental tracers (Worthington & Gunn, 2009). Therefore, it is necessary to understand the intrinsic characteristics of the media, as they can affect the interpretation of groundwater dating data.

The geological complexity of the Jarastepar aquifer, and particularly the existence of a major tectonic contact with imbrication of impervious materials (Flysch), together with the great thickness of the semi-confined Jurassic and Triassic calcareous formations, confer the springs placed in the IZ of the aquifer lagged and buffer responses to precipitation events (Fig. 3). That is the typical behavior showed by springs draining carbonate aquifers with dominated fissured or diffuse flow functioning (Jeannin, Groves, & Hauselmann, 2007; Mudarra & Andreo, 2011; Perrin et al., 2003). However, the mean ages estimated in this case nearly reach the century

(Tab. 4) instead of a few years or decades, as it normally occurs in other small alpine karst aquifers (Althaus et al., 2009; Lauber & Goldscheider, 2014). Besides, the models suggest that an old flow component with mean residence times around 200 years exists (Tab. 4). This kind of binary mixing, including centennial groundwater, is normally observed in large carbonate aquifers that often are partially confined (Jiang et al., 2019; Toth & Katz, 2006; Yager et al., 2010; Zang et al., 2015). However, the Jarastepar aquifer is far from that definition, as its outcropping surface is 56 km^2 and most of it corresponds to the unconfined EZ, which can be rapidly drained through the overflow springs. The distance from the tectonic suture to the perennial outlets is short, particularly in the southwest, where the overflow area is 600 m far from Huertos spring (Fig. 1). Assuming a straight-forward flow connecting both points, groundwater should have a velocity of 6 m/year, as the mean residence time of the groundwater drained by Huertos spring is estimated in nearly 100 years (Tab. 4), and the groundwater drained through the overflow springs is infiltrated only a few hours before. Such flow velocities do not seem reasonable in karst formations.

Based on geological observations and hydrogeological methods (hydrochemistry, hydrodynamics, stable isotopes), De la Torre et al. (2020) proposed a hydrogeological conceptual model of the aquifer that helps to understand the presence of old groundwater. The existence of imbricated layer (discontinuous because of tectonic reasons) between the EZ and the IZ, formed by Flysch-type clays and sandstones and Cretaceous-Tertiary marls and marly limestones, slow down the transference of groundwater from the Jurassic carbonate formation (EZ) to the Triassic dolomites (IZ). That groundwater comes from the saturated zone and is older than that drained through the overflow springs (Fig. 8). Additionally, the flow deceleration produced by the los permeability formations would lead to a greater residence time of groundwater within the media. All that combined would explain the existence of young groundwater components in the permanent springs with mean transit times of few decades (Tab. 4 and Fig. 6).

The presence of an old groundwater flow component can be attributable to the combined thickness of the Jurassic and the Triassic carbonate formations, which could reach 1000 m. Both units are partially confined bellow the metamorphic formations of the IZ and their extension southwards is unknown. Furthermore, the karstification degree and the permeability of the dolostones of the IZ are lower than in the EZ. In any case, groundwater only can leave the system through the perennial springs. Thus, after groundwater traverses a long flowpath to deep areas of the aquifer, the tectonic contact with the low permeable rocks forces the ascent of the groundwater flow towards the outlets (Fig. 8). According to the low values of water temperature (Tab. 1), the upwelling through the Triassic dolomite formation must occur slowly, allowing a greater transference of Mg^{2+} to groundwater and the temperature re-equilibrium. That explains why the correlation of groundwater age parameters with rMg/Ca is high while it is lower with SO_4^{2-} (Fig. 7).

These findings not only demonstrate the existence of centennial groundwater in a realtively small alpine karst aquifer, but they also show how the particularities of the geological framework can greatly affect the flow dynamics and the residence time of groundwater. There is little evidence of centennial groundwater in this type of system except for some karst springs in the Austrian Alps that drain deep reservoirs connected to major faults (Han et al., 2007; Hilberg & Schneider, 2011). The fact that groundwater age in alpine karst can be this old has great implications in the hydrogeological management, but also regarding its intrinsic vulnerability to pollution. Therefore, contrary to what is expected, the complementary use of environmental dating tracers and hydrochemistry in complex carbonate formations can be useful for the management of its groundwater resources, particularly if the structure of the aquifer is complex.

CONCLUSIONS

In this research work, conventional hydrogeological methods used in karst aquifer studies (hydrochemistry, hydrodynamics, and water temperature) were jointly applied with groundwater dating tools (^3H, ^3He, ^4He, CFC-12, CFC-11, and SF_6) to explain the functioning of a complex and relatively small alpine karst aquifer. Based on the environmental-tracer concentrations, Lumped Parameter Models and Free-Shape Models were created to define the groundwater-age distribution of the springs water under different hydrodynamic conditions. All that permitted to identify the existence of two main flow components in the mix drained through the springs and to assed their groundwater age distribution. This kind of binary mixing is coherent with

karst systems in which conduit flow and diffuse flow coexist. However, in these cases, the mean ages of the springs are several decades old, and the old component could have approximately 200 years. Those transit times are large for a relatively small alpine karst area but here can be explained by a complex geological setting, including a major tectonic contact that involves low permeability material imbricated and a thick semiconfined saturated zone.

The hydrochemical characteristics of the springs, and particularly the rise of mineralization and the rMg/Ca values towards lower altitudes, are compatible with large residence times. Besides, the natural responses registered in the spring waters, including the variations in contents of the radiogenic ^{4}He, are coherent with the described binary mixing. In that sense, despite the number of analyzed samples was limited, the study of the evolution of environmental tracer concentration in the water of karst spring may be a useful tool in future works to help with their hydrogeological understanding.

The results here presented demonstrate the applicability of using environmental dating tracers in karst areas located in alpine mountains, and show their usefulness on the interpretation of hydrogeological functioning when combined with hydrochemical data and natural response analysis. Therefore, this methodological approach is potentially useful in other alpine karst aquifers of complex geology. In that way, the age distribution of the groundwater drained through karst spring can be understood, which is crucial for the assessment of pollution vulnerability and the definition of safeguard zones for groundwater protection.

REFERENCES

Aeschbach-Hertig, Peeters, F., Beyerle, U., & Kipfer, R. (1999). Interpretation of dissolved atmospheric noble gases in natural waters. *Water Resources Research* , *35* (9), 2779–2792.

Akesson, M., Suckow, A., Visser, A., Sultenfuss, J., Laier, T., Purtschert, R., & Sparrenbom, C. J. (2015). Constraining age distributions of groundwater from public supply wells in diverse hydrogeological settings in Scania, Sweden. *Journal of Hydrology* ,*528* , 217–229. https://doi.org/10.1016/j.jhydrol.2015.06.022

Althaus, R., Klump, S., Onnis, A., Kipfer, R., Purtschert, R., Stauffer, F., & Kinzelbach, W. (2009). Noble gas tracers for characterisation of flow dynamics and origin of groundwater: A case study in Switzerland. *Journal of Hydrology* , *370* (1–4), 64–72. https://doi.org/10.1016/j.jhydrol.2009.02.053

Appelo, C. A. J., & Postma, D. (2005). *Geochemistry, Groundwater, and Pollution* (2nd ed.). Amsterdam: A.A. Balkema publishers.

Ballesteros, D., Jimenez-Sanchez, M., Giralt, S., Garcia-Sansegundo, J., & Melendez-Asensio, M. (2015). A multi-method approach for speleogenetic research on alpine karst caves. Torca La Texa shaft, Picos de Europa (Spain). *Geomorphology* , *247* , 35–54. https://doi.org/10.1016/j.geomorph.2015.02.026

Barbera, J. A., Mudarra, M., Andreo, B., & De la Torre, B. (2018). Regional-scale analysis of karst underground flow deduced from tracing experiments: examples from carbonate aquifers in Malaga province, southern Spain. *Hydrogeology Journal* , *26* (1), 23–40. https://doi.org/10.1007/s10040-017-1638-5

Beyerle, U., Aeschbach-Hertig, W., Hofer, M., Imboden, D. M., Baur, H., & Kipfer, R. (1999). Infiltration of river water to a shallow aquifer investigated with H-3/He-3, noble gases, and CFCs. *Journal of Hydrology* , *220* (3–4), 169–185.

Birk, S., Liedl, R., & Sauter, M. (2004). Identification of localised recharge and conduit flow by combined analysis of hydraulic and physico-chemical spring responses (Urenbrunnen, SW-Germany). *Journal of Hydrology* , *286* (1–4), 179–193. https://doi.org/10.1016/j.jhydrol.2003.09.007

Bullister, J. L., & Tanhua, T. (2010). Sampling and Measurement of Chlorofluorocarbons and Sulfur. In E. Hood, C. L. Sabne, & B. Sloyan (Eds.), *The GO-SHIP repeat hydrography manual: a collection of expert reports and guidelines* . IOCCP Report Number 14, ICPO Public ation Series Number 134.

Bulsiewicz, K., Rose, H., Klatt, O., Putzka, A., & Roether, W. (1998). A capillary-column chromatographic system for efficient chlorofluorocarbon measurement in ocean waters. *Journal of Geophysical Research* , *103*

(C8), 15959–15970. https://doi.org/10.1029/98JC00140

Busenberg, E., & Plummer, L. N. (2000). Dating young groundwater with sulfur hexafluoride: Natural and anthropogenic sources of sulfur hexafluoride. *Water Resources Research* , *36* (10), 3011–3030.

Carucci, V., Petitta, M., & Aravena, R. (2012). Interaction between shallow and deep aquifers in the Tivoli Plain (Central Italy) enhanced by groundwater extraction: A multi-isotope approach and geochemical modeling. *Applied Geochemistry* , *27* (1), 266–280. https://doi.org/10.1016/j.apgeochem.2011.11.007

Chenini, I., Farhat, B., & Ben Mammou, A. B. (2010). Identification of major sources controlling groundwater chemistry from a multilayered aquifer system. *Chemical Speciation and Bioavailability* ,*22* (3), 183–189. https://doi.org/10.3184/095422910X12829228276711

Clarke, W. B., Jenkins, W. J., & Top, Z. (1976). Determination of tritium by mass spectrometric measurement of ^{3}He.*International Journal of Applied Radiation and Isotopes* ,*27* (9), 515–522.

Cook, P., Solomon, D. K., Sanford, W. E., Busenberg, E., & Plummer, L. N. (1996). Inferring shallow groundwater flow in saprolite and fractured rock using environmental tracers. *Water Resources Research* ,*32* (6), 1501–1509.

Cook, P. G., & Solomon, D. K. (1997). Recent advances in dating young groundwater: Chlorofluorocarbons,^{3}H/^{3}He and ^{85}Kr.*Journal of Hydrology* , *191* (1–4), 245–265. https://doi.org/10.1016/S0022-1694(96)03051-X

Cook, P. G., & Herczeg, A. L. (2000). *Environmental Tracers in Subsurface Hydrology* . (Peter G. Cook & A. L. Herczeg, Eds.),*Book* . New York: Springer Science/Business Media. https://doi.org/10.1017/CBO9781107415324.004

Corcho Alvarado, J. A., Purtschert, R., Barbecot, F., Chabault, C., Rueedi, J., Schneider, V., Aeschbach-Hertig, W., Kipfer, R. & Loosli, H. H. (2007). Constraining the age distribution of highly mixed groundwater using ^{39}Ar: A multiple environmental tracer (^{3}H/^{3}He,^{85}Kr, ^{39}Ar, and^{14}C) study in the semiconfined Fontainebleau Sands Aquifer. *Water Resources Research* , *43* (3), 1–16. https://doi.org/10.1029/2006WR005096

De la Torre, B. (2020). Uso conjunto de trazadores naturales y artificiales para determinar el funcionamiento hidrogeologico del macizo carbonatico de la sierra de Jarastepar y sectores adyacentes (provincia de Malaga). PhD Thesis, Univ. de Jaen, 540 pp.

De la Torre, B., Mudarra, M., & Andreo, B. (2020). Investigating karst aquifers in tectonically complex alpine areas coupling geological and hydrogeological methods. *Journal of Hydrology X* ,*6* (November 2019), 100047. https://doi.org/10.1016/j.hydroa.2019.100047

Delbart, C., Barbecot, F., Valdes, D., Tognelli, A., Fourre, E., Purtschert, R., Couchoux, L. & Jean-Baptiste, P. (2014). Investigation of young water inflow in karst aquifers using SF_6-CFC-^{3}H/He-^{85}Kr-^{39}Ar and stable isotope components. *Applied Geochemistry* , *50* , 164–176. https://doi.org/10.1016/j.apgeochem.2014.01.011

Ebrahimi, B., Pasandi, M., & Ahmadipour, M. R. (2007). Hydrodynamic behaviour of karstic aquifers in Boroujerd, western Iran.*Hydrological Sciences Journal* , *52* (1), 192–205. https://doi.org/10.1623/hysj.52.1.192

Elliot, T. (2014). Environmental tracers. *Water (Switzerland)* ,*6* (11), 3264–3269. https://doi.org/10.3390/w6113264

Field, M. S. S. (1999). *A Lexicon of Cave and Karst Terminology with Special Reference to Environmental Karst Hydrology* . (U. E. P. Agency, Ed.), *Environmental Protection* . Washington, D.C.: US Environmental Protection Agency. Retrieved from http://www.vnovak.hr/speleo/znanost/terminologija/glossary.pdf

Ford, D. C. (1983). Alpine karst systems at Crowsnest Pass, Alberta-British Columbia, Canada. *Journal of Hydrology* ,*61* , 187–192.

Gardner, P. M., & Heilweil, V. M. (2014). A multiple-tracer approach to understanding regional groundwater flow in the Snake Valley area of the eastern Great Basin, USA. *Applied Geochemistry* , *45* , 33–49. https://doi.org/10.1016/j.apgeochem.2014.02.010

Gil-Marquez, J. M., Sultenfuss, J., Andreo, B., & Mudarra, M. (2020). Groundwater dating tools (^{3}H, ^{3}He,^{4}He, CFC-12, SF_6) coupled with hydrochemistry to evaluate the hydrogeological functioning of complex evaporite-karst settings. *Journal of Hydrology* , *580* (May 2019), 124263. https://doi.org/10.1016/j.jhydrol.2019.124263

Goldscheider, N., & Drew, D. (2007). *Methods In Karst Hydrogeology* . London: Taylor & Francis.

Hamill, L. & Bell, F. G. (1986). *Groundwater resource development* . Butterworth, London; Boston

Han, L., Hacker, P., & Groning, M. (2007). Residence times and age distributions of spring waters at the Semmering catchment area, Eastern Austria, as inferred from tritium, CFCs and stable isotopes.*Isotopes in Environmental and Health Studies* , *43* (1), 31–50. https://doi.org/10.1080/10256010601154015

Hilberg, S., & Schneider, J. F. (2011). The Aquifer Characteristics of the Dolomite Formation a New Approach for Providing Drinking Water in the Northern Calcareous Alps Region in Germany and Austria. *Water Resources Management* , *25* (11), 2705–2729. https://doi.org/10.1007/s11269-011-9834-x

IAEA/WMO, 2019. Global Network of Isotopes in Precipitation. The GNIP Database. [WWW Document]. https://nucleus.iaea.org/wiser/index.aspx.

IAEA. (2006). *Use of Chlorofluorocarbons in Hydrology: a guidebook* . *International Atomic Energy Agency* . Vienna: International Atomic Energy Agency. Retrieved from http://scholar.google.com/scholar?hl=en&btnG=Search&q=intitle:Use+of+chlorofluorocarbons+in+hydrology#2

Jasechko, S., Perrone, D., Befus, K. M., Bayani Cardenas, M., Ferguson, G., Gleeson, T., Luijendijk, E., McDonell, J.J., Taylor, R.G., Wada, Y. & Kirchner, J. W. (2017). Global aquifers dominated by fossil groundwaters but wells vulnerable to modern contamination. *Nature Geoscience* , (April), 1–6. https://doi.org/10.1038/ngeo2943

Jaunat, J., Huneau, F., Dupuy, A., Celle-Jeanton, H., Vergnaud-Ayraud, V., Aquilina, L., Labasque, T. & Le Coustumer, P. (2012). Hydrochemical data and groundwater dating to infer differential flowpaths through weathered profiles of a fractured aquifer. *Applied Geochemistry* ,*27* (10), 2053–2067. https://doi.org/10.1016/j.apgeochem.2012.06.009

Jeannin, P. Y., Groves, C., & Hauselmann, P. (2007). Speleological investigations. In N. Goldscheider & D. Drew (Eds.), *Methods in karst hydrogeology* (pp. 25–44). London: Taylor & Francis.

Jiang, G., Guo, F., & Tang, C. (2019). Groundwater systems in bare and covered karst aquifers: evidence from tracer tests, hydrochemistry, and groundwater ages. *Environmental Earth Sciences* , *78* (20), 1–14. https://doi.org/10.1007/s12665-019-8622-4

Jurgens, B. C., Bohlke, J. K., Eberts, S. M., & Survey, U. S. G. (2012). TracerLPM (Version 1): An Excel(r) workbook for interpreting groundwater age distributions from environmental tracer data.*Techniques and Methods* , (Version 1). Retrieved from http://pubs.er.usgs.gov/publication/tm4F3

Koh, E. H., Lee, E., Kaown, D., Green, C. T., Koh, D. C., Lee, K. K., & Lee, S. H. (2018). Comparison of groundwater age models for assessing nitrate loading, transport pathways, and management options in a complex aquifer system. *Hydrological Processes* , *32* (7), 923–938. https://doi.org/10.1002/hyp.11465

Land, L., & Huff, G. F. (2010). Multi-tracer investigation of groundwater residence time in a karstic aquifer: Bitter Lakes National Wildlife Refuge, New Mexico, USA. *Hydrogeology Journal* ,*18* (2), 455–472. https://doi.org/10.1007/s10040-009-0522-3

Lauber, U., & Goldscheider, N. (2014). Use of artificial and natural tracers to assess groundwater transit-time distribution and flow systems in a high-alpine karst system (Wetterstein Mountains, Germany).*Hydrogeology*

Journal , *22* (8), 1807–1824. https://doi.org/10.1007/s10040-014-1173-6

Lehmann, B. E., Love, A., Purtschert, R., Collon, P., Loosli, H. H., Kutschera, W., Beyerle, U., Aeschbach-Hertig, W., Kipfer, R, Frape, S.K., Herczeg, A., Moran, J., Tolstinkhin, I.N., & Groning, M. (2003). A comparison of groundwater dating with ^{81}Kr,^{36}Cl, and ^{4}He in four wells of the Great Artesian Basin, Australia. *Earth and Planetary Science Letters* , *211* (3–4), 237–250. https://doi.org/10.1016/S0012-821X(03)00206-1

Long, A. J., & Putnam, L. D. (2009). Age-distribution estimation for karst groundwater: Issues of parameterization and complexity in inverse modeling by convolution. *Journal of Hydrology* , *376* (3–4), 579–588. https://doi.org/10.1016/j.jhydrol.2009.07.064

Lucas, L., & Unterweger, M. (2000). Comprehensive review and critical evaluation of the half-life of tritium. *Journal of Research of the National Institute of Standards and Technology* , *105* (4), 541. https://doi.org/10.6028/jres.105.043

Maloszewski, P., & Zuber, A. (1982). Determining the turnover time of groundwater systems with the aid of environmental tracers. *Journal of Hydrology* , *57* , 207–231.

Martin-Algarra, A., 1987. *Evolucion geologica alpina del contacto entre las Zonas Internas y las Externas de la Cordillera Betica* . PhD Thesis. University of Granada (Spain). 1171 pp.

Mayer, A., Sultenfuss, J., Travi, Y., Rebeix, R., Purtschert, R., Claude, C., Le Gal La Salle, C., Miche, H. & Conchetto, E. (2014). A multi-tracer study of groundwater origin and transit-time in the aquifers of the Venice region (Italy). *Applied Geochemistry* ,*50* , 177–198. https://doi.org/10.1016/j.apgeochem.2013.10.009

McMahon, P. B., Bohlke, J. K., & Christenson, S. C. (2004). Geochemistry, radiocarbon ages, and paleorecharge conditions along a transect in the central High Plains aquifer, southwestern Kansas, USA. *Applied Geochemistry* , *19* (11), 1655–1686. https://doi.org/10.1016/j.apgeochem.2004.05.003

Moral, F., Cruz-Sanjulian, J. J., & Olias, M. (2008). Geochemical evolution of groundwater in the carbonate aquifers of Sierra de Segura (Betic Cordillera, southern Spain). *Journal of Hydrology* ,*360* (1–4), 281–296. https://doi.org/10.1016/j.jhydrol.2008.07.012

Mudarra, M., & Andreo, B. (2011). Relative importance of the saturated and the unsaturated zones in the hydrogeological functioning of karst aquifers: The case of Alta Cadena (Southern Spain). *Journal of Hydrology* , *397* (3–4), 263–280. https://doi.org/10.1016/j.jhydrol.2010.12.005

Muller, T., Osenbruck, K., Strauch, G., Pavetich, S., Al-Mashaikhi, K. S., Herb, C., Merchel, S., Rugel, G., Aeschbach, W. & Sanford, W. (2016). Use of multiple age tracers to estimate groundwater residence times and long-term recharge rates in arid southern Oman. *Applied Geochemistry* , *74* , 67–83. https://doi.org/10.1016/j.apgeochem.2016.08.012

Musgrove, M., Solder, J. E., Opsahl, S. P., & Wilson, J. T. (2019). Timescales of water-quality change in a karst aquifer, south-central Texas. *Journal of Hydrology X* , *4* (July), 100041. https://doi.org/10.1016/j.hydroa.2019.100041

Palmer, A. N. (1984). Objectives and current status of alpine and arctic karst research. *Norsk Geografisk Tidsskrift* , *38* (3–4), 145–150. https://doi.org/10.1080/00291958408552118

Perrin, J., Jeannin, P. Y., & Zwahlen, F. (2003). Implications of the spatial variability of infiltration-water chemistry for the investigation of a karst aquifer: A field study at Milandre test site, Swiss Jura. *Hydrogeology Journal* , *11* (6), 673–686. https://doi.org/10.1007/s10040-003-0281-5

Plummer, L. N., Busby, J. F., Lee, R. W., & Hanshaw, B. B. (1990). Geochemical Modeling of the Madison Aquifer in Parts of Montana, Wyoming, and South Dakota. *Water Resources Research* ,*26* (9), 1981–2014. https://doi.org/10.1029/WR026i009p01981

Rank, D., Volkl, G., Maloszewski, P., & Stichler, W. (1992). Flow dynamics in an alpine karst massif studied by means of environmental isotopes. *Isotope Techniques in Water Resources Development 1991. Proc. Symposium, Vienna, 1991* , 327–343.

Shah, R. A., Jeelani, G., & Jacob, N. (2017). Estimating mean residence time of karst groundwater in mountainous catchments of Western Himalaya, India. *Hydrological Sciences Journal* , *62* (8), 1230–1242. https://doi.org/10.1080/02626667.2017.1313420

Smart, C. C. (1988). Quantitative tracing of the Maligne karst system, Alberta, Canada. *Journal of Hydrology* , *98* (3–4), 185–204. https://doi.org/10.1016/0022-1694(88)90014-5

Solomon, D. K. (2000). ^{4}He in groundwater. In P.G. Cook & A. L. Herczeg (Eds.), *Environmental tracers in subsurface hydrology* . Springer Science+Business Media.

Spangler, L. E. (2001). Delineation of Recharge Areas for Karst Springs in Logan Canyon. In E. L. Kumiansky (Ed.), *U.S. Geological Survey Karst Interest Group Proceedings, Water-Resources Investigations Report 01-4011* (pp. 186–193).

Suckow, A. (2014). The age of groundwater - Definitions, models and why we do not need this term. *Applied Geochemistry* , *50* , 222–230. https://doi.org/10.1016/j.apgeochem.2014.04.016

Sultenfuss, J., Purtschert, R., & Fuhrboter, J. F. (2011). Age structure and recharge conditions of a coastal aquifer (northern Germany) investigated with ^{39}Ar,^{14}C, ^{3}H, He isotopes and Ne.*Hydrogeology Journal* , *19* , 221–236. https://doi.org/10.1007/s10040-010-0663-4

Sultenfuss, J., Roether, W., & Rhein, M. (2009). The Bremen mass spectrometric facility for the measurement of helium isotopes, neon, and tritium in water. *Isotopes in Environmental and Health Studies* ,*45* (2), 83–95. https://doi.org/10.1080/10256010902871929

Torgersen, T., Clarke, W. B., & Jenkins, W. J. (1978). The tritium/helium-3 method in hydrology. In *Isotope Hydrology 1978, IAEA Symposium* . Neuherberg, Germany.

Toth, D. J., & Katz, B. G. (2006). Mixing of shallow and deep groundwater as indicated by the chemistry and age of karstic springs.*Hydrogeology Journal* , *14* (5), 827–847. https://doi.org/10.1007/s10040-005-0478-x

Turk, J., Malard, A., Jeannin, P. Y., Petrič, M., Gabrovšek, F., Ravbar, N., ... Sordet, V. (2015). Hydrogeological characterization of groundwater storage and drainage in an alpine karst aquifer (the Kanin massif, Julian Alps). *Hydrological Processes* , *29* (8), 1986–1998. https://doi.org/10.1002/hyp.10313

USGS. (2018). Atmospheric mixing ratios of CFC-11, CFC-12, CFC-113, SF_6 x100, and tritium in precipitations for Northern Hemisphere atmosphere.

Visser, A., Broers, H. P., Purtschert, R., Sültenfuß, J., & de Jonge, M. (2013). Groundwater age distributions at a public drinking water supply well field derived from multiple age tracers (^{85}Kr, ^{3}H/^{3}He, and^{39}Ar). *Water Resources Research* , *49* (11), 7778–7796. https://doi.org/10.1002/2013WR014012

Werner, E. (1979). Alpine Karst in the Rocky Mountains. *Quarterly Journal of the National Speleological Society* , *41* (3), 51–52. https://doi.org/10.1017/CBO9781107415324.004

Wigley, T. M. L. (1973). The incongruent solution of dolomite.*Geochimica et Cosmochimica Acta* , *37* (5), 1397–1402. https://doi.org/10.1016/0016-7037(73)90072-0

Wilske, C., Suckow, A., Mallast, U., Meier, C., Merchel, S., Merkel, B., Pavetich, S., Rödiger, T., Rugel, G., Saches, A., Weise, S. M. & Siebert, C. (2019). A multi-environmental tracer study to determine groundwater residence times and recharge in a structurally complex multi-aquifer system. *Hydrology and Earth System Sciences Discussions* , (September), 1–30. https://doi.org/10.5194/hess-2019-451

Worthington, S. R. H., & Gunn, J. (2009). Hydrogeology of carbonate aquifers: A short history. *Ground Water* , *47* (3), 462–467. https://doi.org/10.1111/j.1745-6584.2008.00548.x

Wu, P., Shu, L., Li, F., Chen, H., Xu, Y., & Zou, Z. (2019). Impacts of Artificial Regulation on Karst Spring. *Water* , *11* , 755.

Xanke, J., Goeppert, N., Sawarieh, A., Liesch, T., Kinger, J., Ali, W., Hötzl, H., Hadidi, K. & Goldscheider, N. (2015). Impact of managed aquifer recharge on the chemical and isotopic composition of a karst aquifer, Wala reservoir, Jordan. *Hydrogeology Journal* ,*23* (5), 1027–1040. https://doi.org/10.1007/s10040-015-1233-6

Xu, N., Gong, J., & Yang, G. (2018). Using environmental isotopes along with major hydro-geochemical compositions to assess deep groundwater formation and evolution in eastern coastal China. *Journal of Contaminant Hydrology* , *208* (November 2017), 1–9. https://doi.org/10.1016/j.jconhyd.2017.11.003

Yager, R. M., Plummer, L. N., Kauffman, L. J., Doctor, D. H., Nelms, D. L., & Schlosser, P. (2010). Comparison of age distributions estimated from environmental tracers by using binary-dilution and numerical models of fractured and folded karst : Shenandoah Valley of Virginia and West Virginia, USA. *Hydrogeology Journal* , *21* , 1193–1217. https://doi.org/10.1007/s10040-013-0997-9

Zang, H., Zheng, X., Qin, Z., & Jia, Z. (2015). A study of the characteristics of karst groundwater circulation based on multi-isotope approach in the Liulin spring area, North China. *Isotopes in Environmental and Health Studies* , *51* (2), 271–284. https://doi.org/10.1080/10256016.2015.987275

Table 1. Statistical parameters of flow rate, electrical conductivity (EC), water temperature (Temp), major ion concentration, and ratio Mg/Ca (rMg/Ca) in the groundwater drained by the main springs of Jarastepar aquifer.

Spring/ Altitude		**Flow rate**	**EC**	**Temp.**	**Alk**	**Ca^{2+}**	**Mg^{2+}**	**SO_4^{2-}**	**rMg/Ca**
(m a.s.l.)		(l/s)	(µS/cm)	(°C)	(mg/l)	(mg/l)	(mg/l)	(mg/l)	
Huertos 560	*n*	99	14735	16890	110	110	110	110	110
	min.	17.6	1747	16.3	214.0	387.3	75.6	991.7	0.11
	max.	32.9	1938	16.9	232.9	484.7	94.2	1309.2	0.13
	mean	**25.5**	**1875**	**16.7**	**226.4**	**437.3**	**87.0**	**1201.1**	**0.12**
	cv (%)	15.1	2.4	0.7	1.5	5.0	3.9	4.8	4.4
Charco 589	*n*	108	15164	15708	126	126	126	126	126
	min.	17.0	1550	15.6	203.7	343.5	58.7	892.3	0.09
	max.	29.7	1707	16.0	222.8	429.2	72.6	1165.1	0.11
	mean	**23.4**	**1673**	**15.8**	**211.2**	**396.1**	**66.0**	**1052.2**	**0.10**
	cv (%)	15.7	1.6	0.7	2.0	4.4	4.2	6.7	4.3
La Zúa 603	*n*	19754	8442	12436	126	126	126	126	126
	min.	149	1540	15.3	190.7	345.0	37.9	834.4	0.06
	max.	298	1591	16.0	226.0	451.4	50.9	1110.5	0.08
	mean	**208**	**1565**	**15.7**	**207.2**	**393.2**	**44.1**	**967.2**	**0.07**
	cv (%)	16.1	0.7	0.7	2.2	5.9	6.6	6.4	2.8
Overflow area 643-664	*n*	897+	19752	19752	198	198	198	198	198
	min.	0.1	260	13.6	165.4	49.6	1.4	1.7	0.02
	max.	21433	494	16.8	309.1	103.3	8.8	18.1	0.10
	mean	**2298**	**352**	**14.9**	**203.5**	**65.4**	**5.1**	**8.3**	**0.05**
	cv (%)	140.0	14.5	4.0	15.7	17.9	29.7	47.3	32.2

+ The number of data of flow-rate in the overflow spring is lower than those of EC and Temp because it can only be measured in high water conditions.

Table 2. Environmental tracer data from the water samples collected at Jarastepar aquifer and derived groundwater date estimations.

Spring	Date of sample	System state	ΔNe (%)	^3H (TU)	$^3He_{trit}$ (TU)	$^4He_{rad}$ (ccSTP/kg)	CFC-12 (pmol/kg)	CFC-11 (pmol/kg)	SF_6 (fmol/kg)	CFC-12 (pptv)	CFC-11 (pptv)	SF_6 (pptv)	Trac ages (yea
													$^3H/$
La Zúa	25/10/14	IW	30.5	2.23	11.7	1.3E-5							33
La Zúa	21/05/15	IW					1.58	2.28		295	111		
La Zúa	29/08/15	LW	39.4	1.94	12	1.5E-5							35
La Zúa	25/05/16	HW					1.30		0.22	243		601	
La Zúa	09/12/16	HW	34.9	1.74	11.9	1.6E-5							36
Charco	25/10/14	IW	27.0	2.46	15.7	2.0E-5							36
Charco	21/05/15	IW					1.04	1.53		195	75		
Charco	29/08/15	LW	34.5	2.06	16.8	2.2E-5							40
Charco	25/05/16	HW					1.11		0.22	209		593	
Charco	09/12/16	HW	26.9	1.9	13.2	1.8E-5							37
Huertos	25/10/14	IW	28.4	2.1	11.6	2.6E-5							33
Huertos	21/05/15	IW					0.98	1.27		184	62		
Huertos	29/08/15	LW	30.7	1.74	12.6	2.3E-5							38
Huertos	25/05/16	HW					0.99		0.17	184		453	
Huertos	09/12/16	HW	27.7	1.65	10.4	2.6E-5							35

LW, IW, and HW refer to low, intermediate and high water hydrodynamic situations. $^+$Ages calculated assuming a $^4He_{rad}$ dissolution rate of $2 \cdot 10^{-7}$ ccSTP·kg^{-1}*yr^{-1}, according to the results of the Lumped Parameter Models.

Table 3. Characteristics of the bins included in the Shape-Free Models (years).

5-bin model	Bin 1	Bin 2	Bin 3	Bin 4	Bin 5 (old bin)
Age range	0-20	20-40	40-60	60-80	80-160 (78-200) $^+$
Mean age	10	30	50	70	120 (140) $^+$
^3H (TU)	2.10	1.64	8.64	0.18	0
$^3He_{trit}$ (TU)	2.5	14.9	101.6	6.9	0
CFC-12 (pptv)	537.2	415.0	98.9	5.7	0
$^4He_{rad}$ (ccSTP/kg)	2.1E-6	6.1E-6	1.0E-5	1.4E-5	2.4E-5

5-bin model	**Bin 1**	**Bin 2**	**Bin 3**	**Bin 4**	**Bin 5 (old bin)**
4-bin model	**Bin 1**	**Bin 2**	**Bin 3**	**Bin 4 (old bin)**	
Bin range	0-26	26-52	52-78	78-160 (78-200) +	
Mean age	13	39	65	119 (136) +	
^{3}H (TU)	1.95	4.15	3.56	0	
$^{3}He_{trit}$ (TU)	5.17	37.86	63.53	0	
CFC-12 (pptv)	533.49	263.473	15.84	0	
Mean age	13	39	65	119 (136) +	

+ Values in brackets are referred only to samples from Huertos spring.

Table 4. Results from groundwater distribution age models. BMM, Binary Mixing Model; PFM, Piston Flow Model; DM, Dispersion Model, SFM, Shape-Free Model; RMSE, Root of the Mean Square Error.

Spring	**Date of sample**	**Sample**	**Sample**	**Sample**	**Sample**	**BMM (**
		^{8}H (TU)	**$^{3}He_{trit}$ (TU)**	**$^{4}He_{rad}$ (ccSTP/kg)**	**CFC-12 (pptv)**	**F_{young} (**
(%)	**F_{young} age**	**Mean age (years)**	**F_{young} (%)**	**F_{young} age**	**F_{old} age**	**GA_{50} (y**
La Zúa	25/10/2014	2.23	11.67	1.3E-05	295	100
La Zúa	09/12/2016	1.74	11.90	1.6E-05	243	87
Charco	25/10/2014	2.46	15.66	2.0E-05	195	70
Charco	09/12/2016	1.90	13.20	1.8E-05	209	69
Huertos	25/10/2014	2.10	11.66	2.6E-05	184	58
Huertos	09/12/2016	1.65	10.40	2.6E-05	184	56

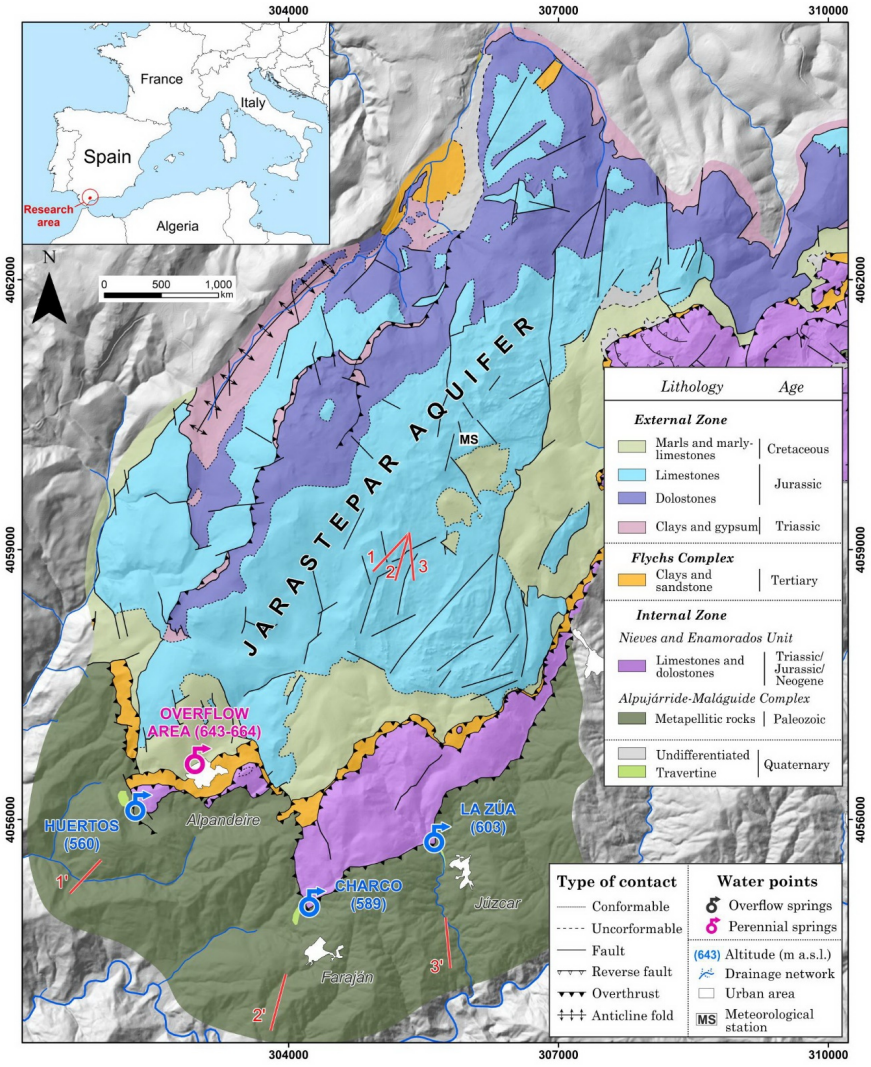

Fig. 1. Geographic location and geological sketch of the Jarastepar mountain range. The cross-sections of figure 2 are indicated.

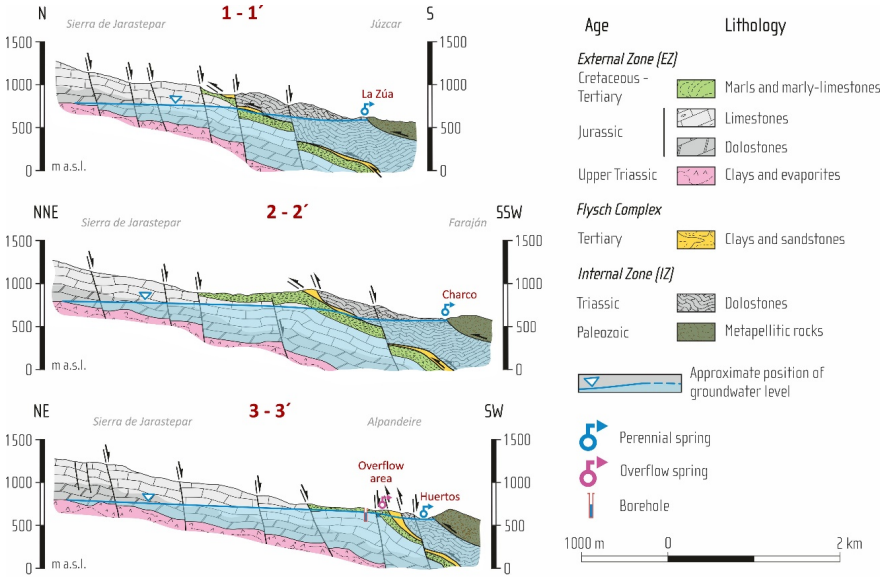

Fig. 2. Geological cross-sections of Jarastepar aquifer. See locations in figure 1.

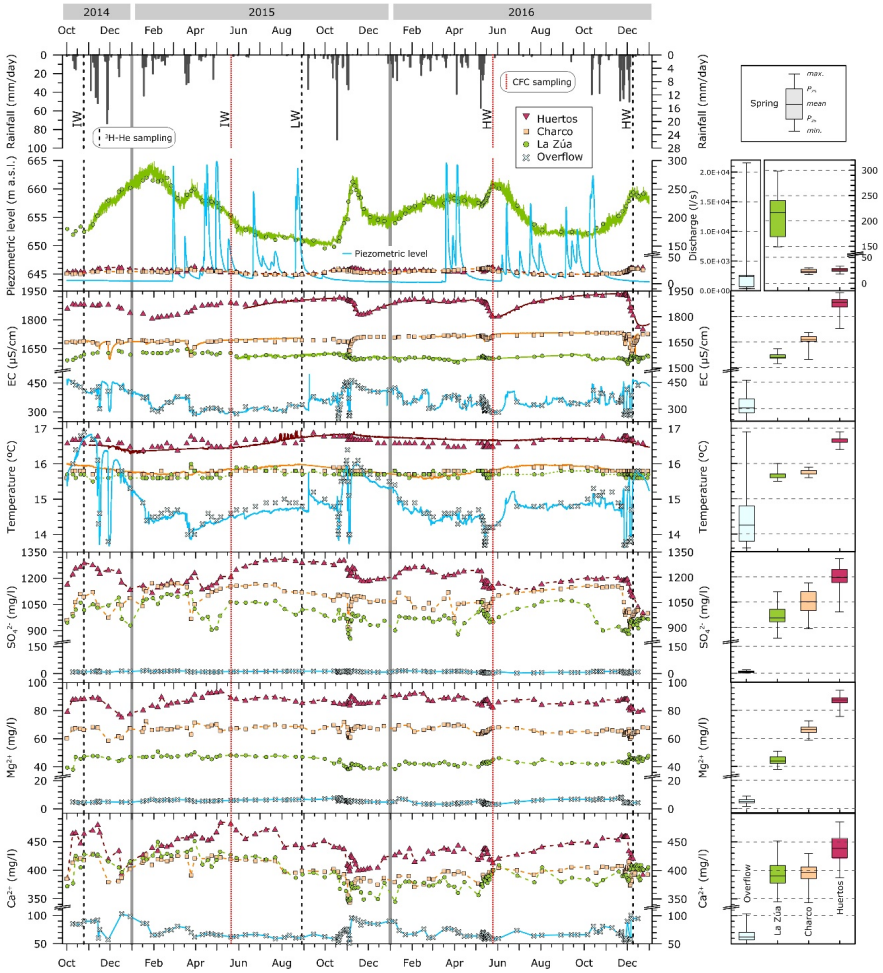

Fig. 3. Temporal evolution and boxplots of Ca^{2+}, Mg^{2+}, SO_4^{2-}, Electrical Conductivity (EC) and water temperature recorded in the groundwater drained through the main outlets of Jarastepar aquifer, from October 2014 to December 2016. The hydrographs of La Zúa, Charco, and Huertos springs are also represented, as well as the limnigraph of the overflow area and the daily rainfall. The sampling campaings for the determination of ^{3}H-He, adn CFC-12, CFC-11, and SF_6 are represented as dashed and dotted lines, respectively. IW, Intermediate water, LW, Low water, HW, high water

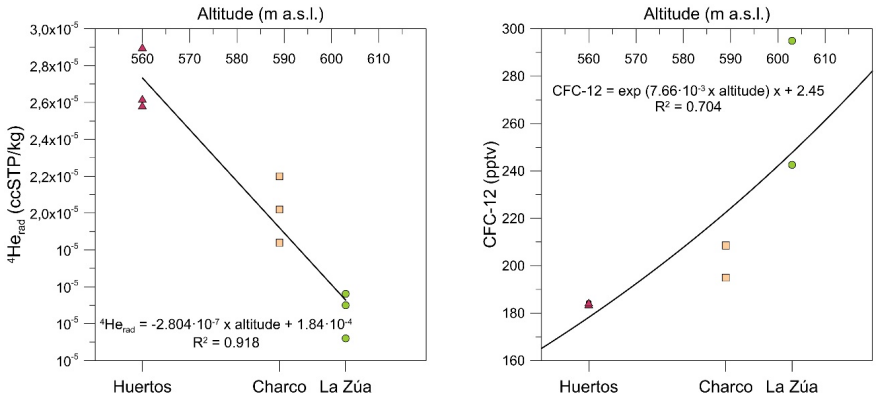

Fig. 4. $^4He_{rad}$ (left) and CFC-12 (right) in the samples and spring heights.

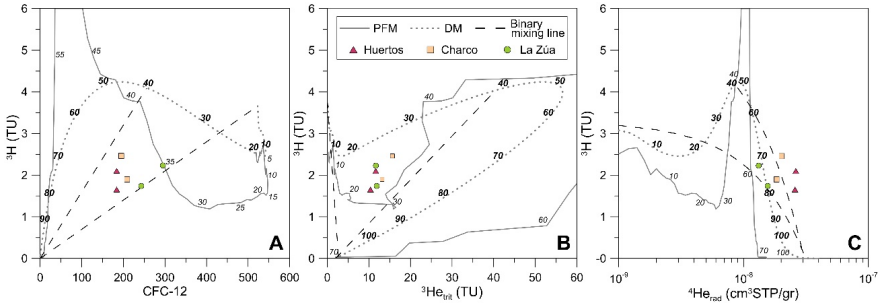

Fig. 5. Tracer-tracer plots comparing measured to modeled tracer concentrations for Piston Flow Model (PFM) and Dispersion Model (DM). Binary mixing lines (0-200 and 40-200 years) are represented, and the age of groundwater is indicated over the model lines.

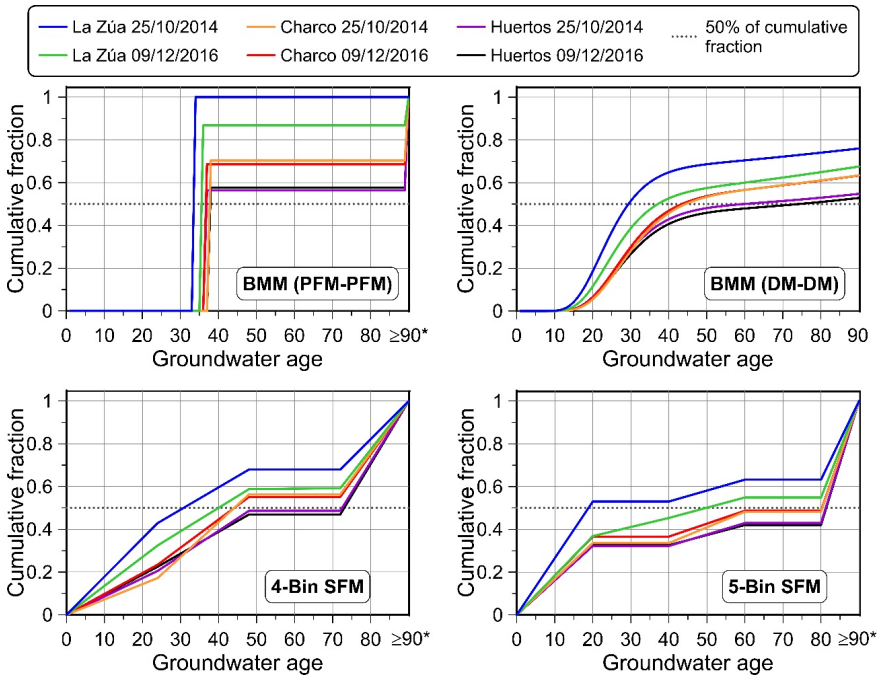

Fig. 6. Cumulative age distribution of the samples described by binary mixing models (BMM) and discrete Shape-Free Models (SFM) of 4 and 5 bins. PFM: Piston Flow Model; DM: Dispersion Model.

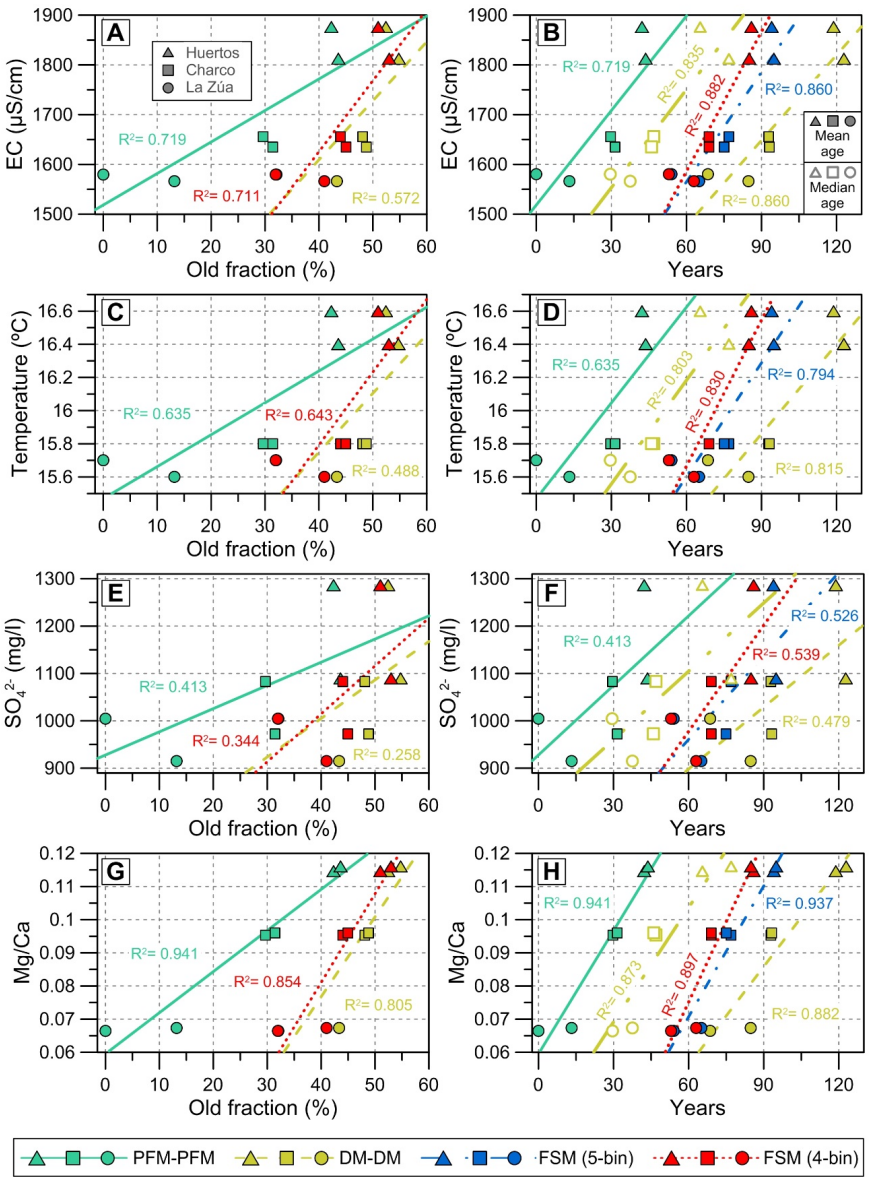

Fig. 7. Electrical Conductivity (EC), water temperature, SO_4^{2-}, and rMg/Ca compared to the percentage of old groundwater component (free of ^3H and CFC-12) deduced from different models (left) and the mean age and the median age (GA_{50}) derived from the BMM DM-DM and the mean age obtained from the 5-bin SFM (right).

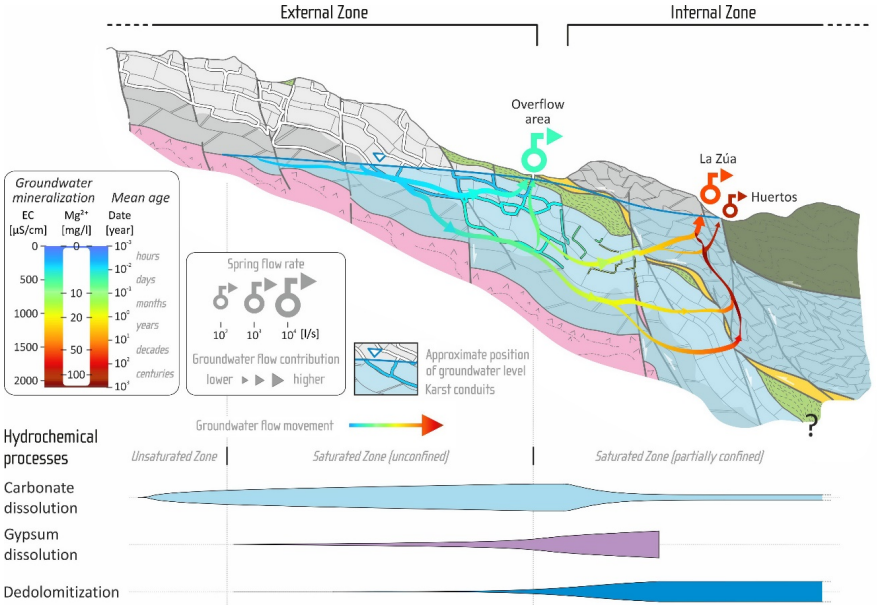

Fig. 8. Hydrogeological conceptual model of Jarastepar aquifer, showing the evolution of EC, Mg^{2+}, and groundwater age, as well as the main geochemical and mixing processes. Lithology explanation in figure 2.

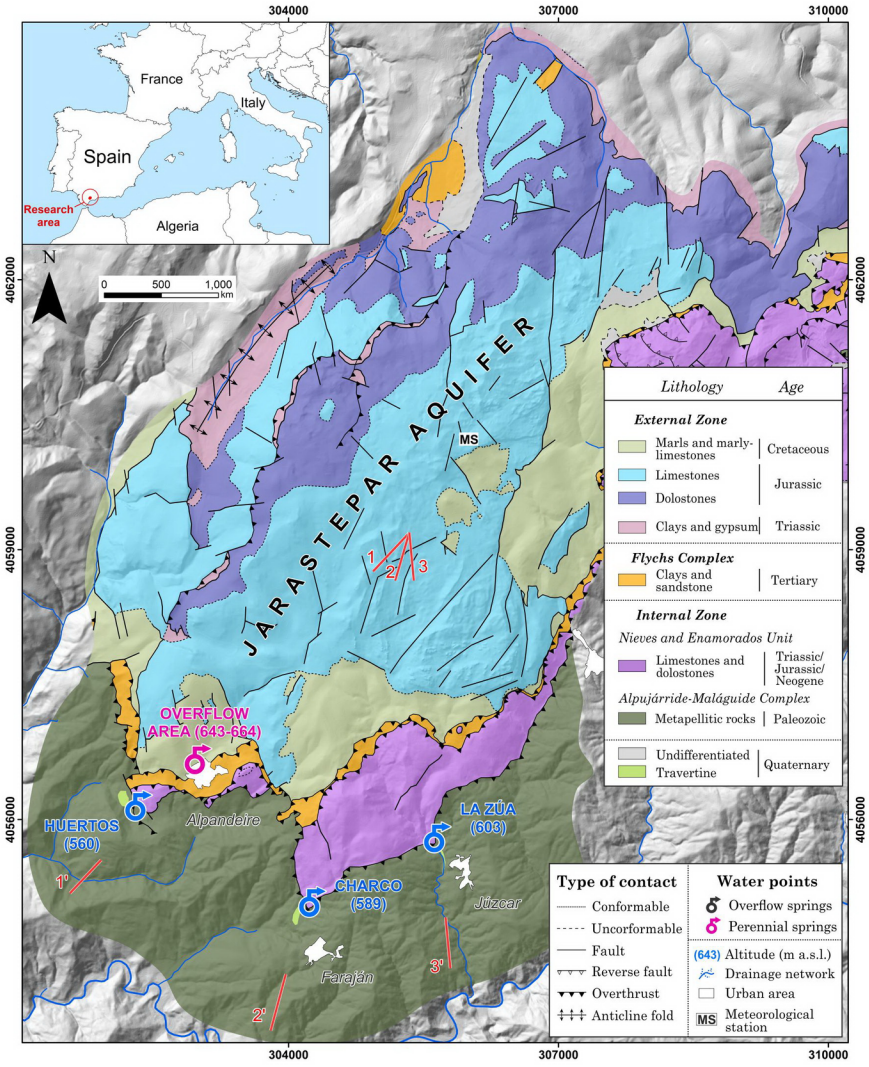

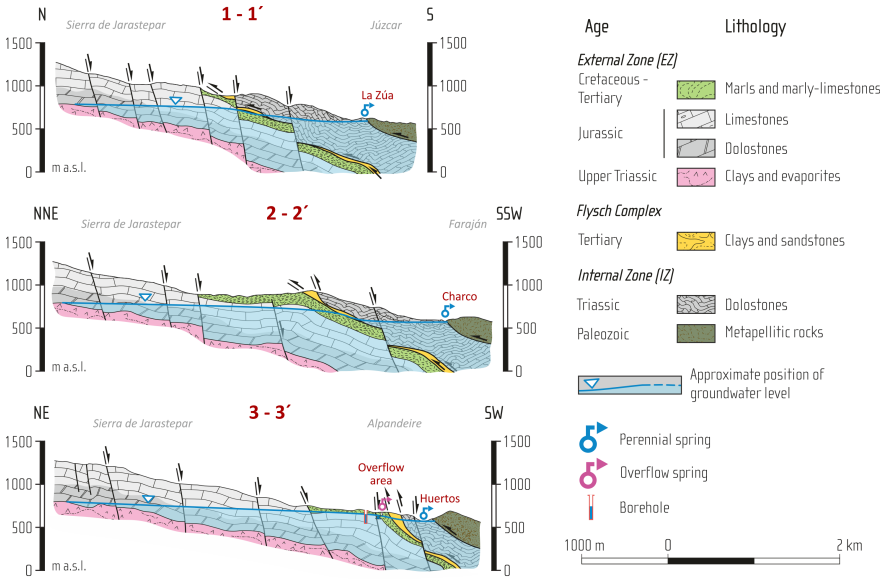

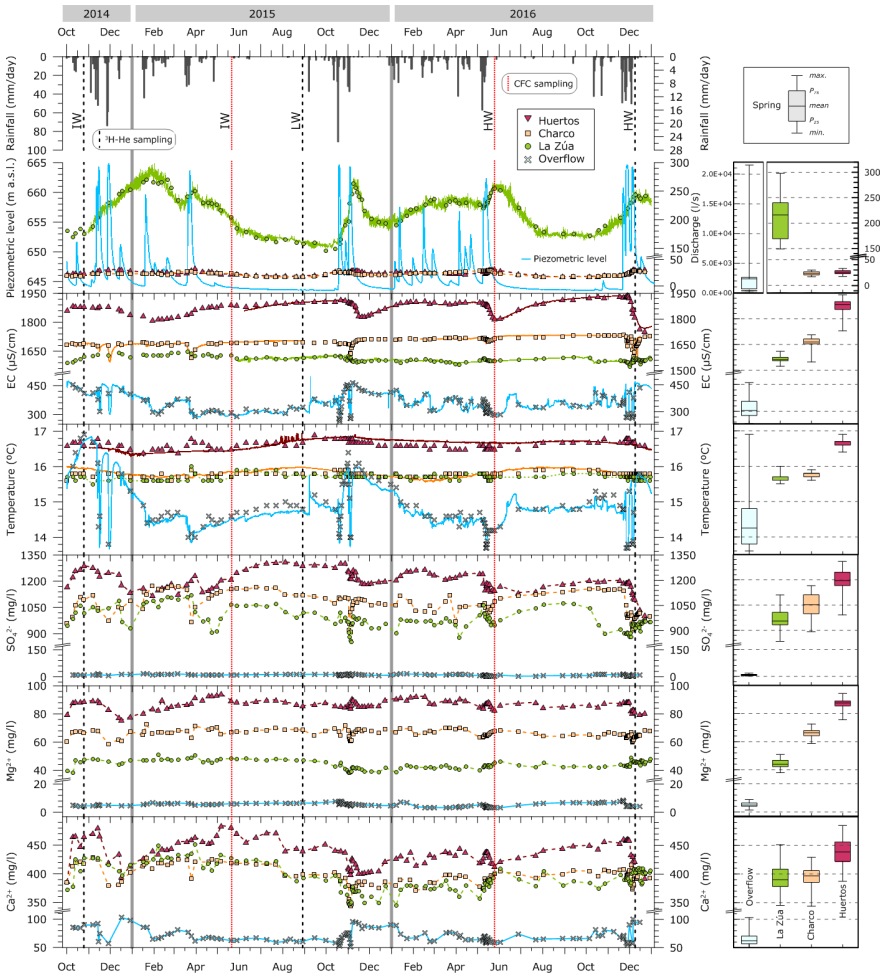

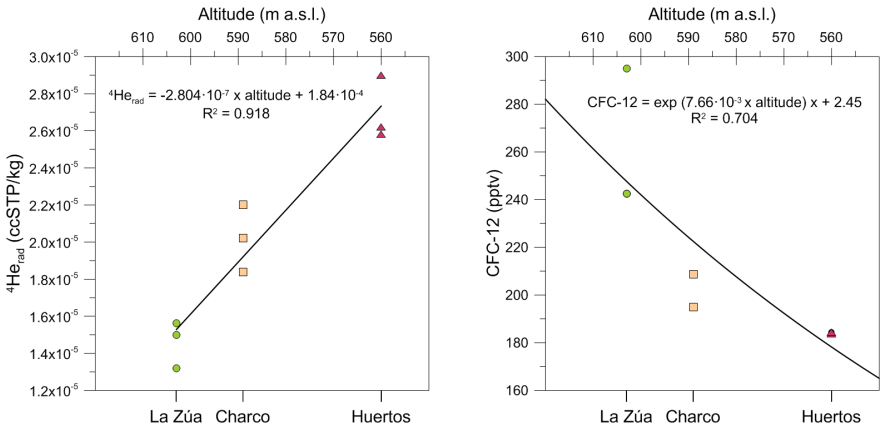

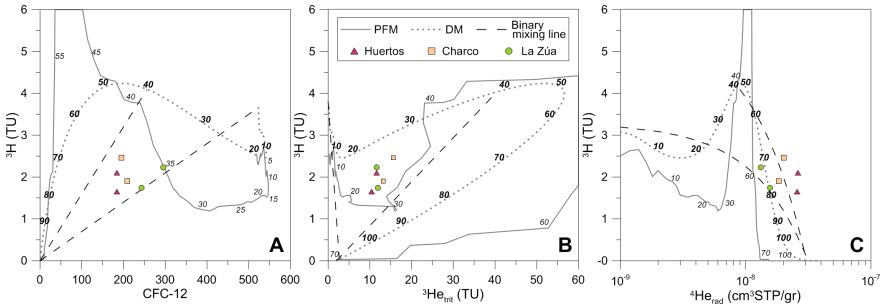

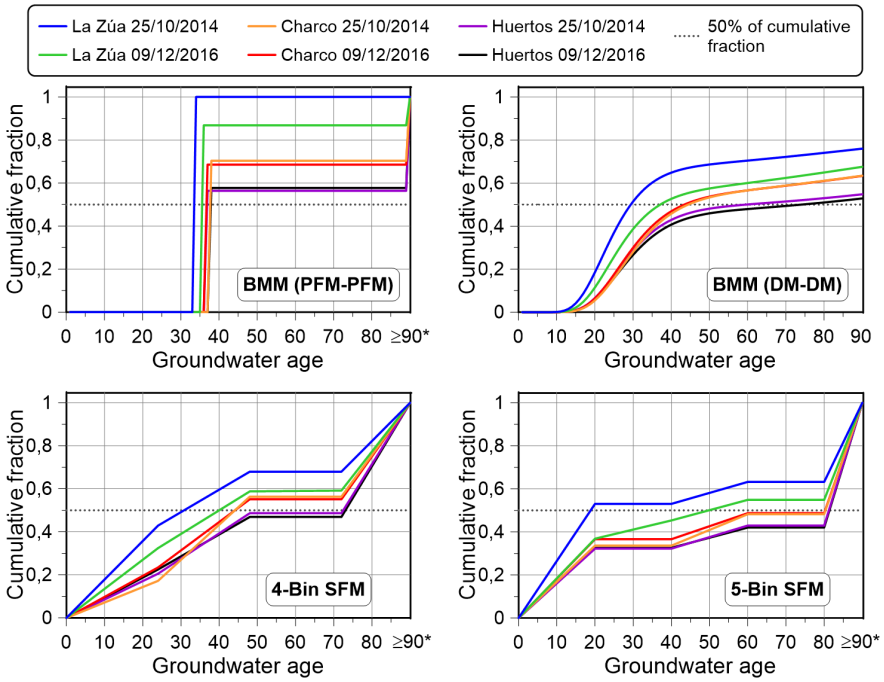

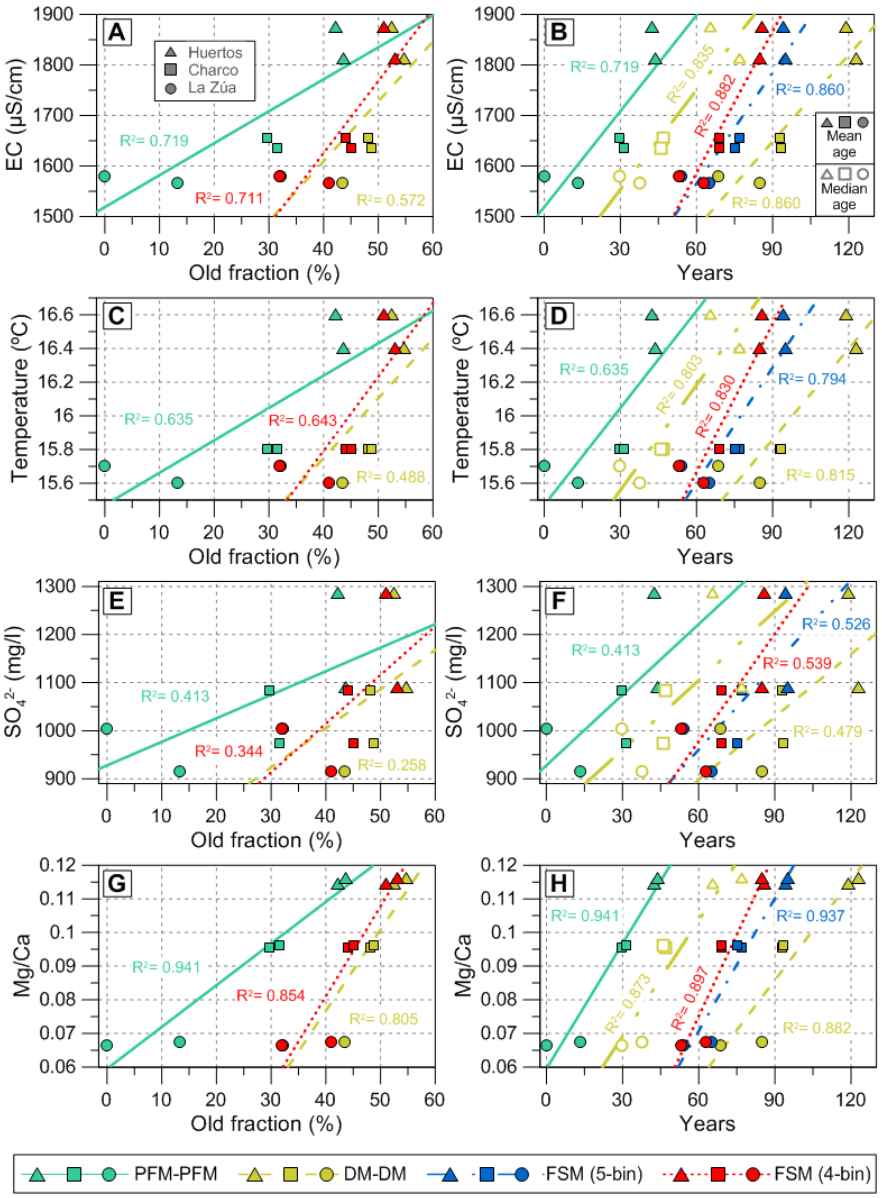

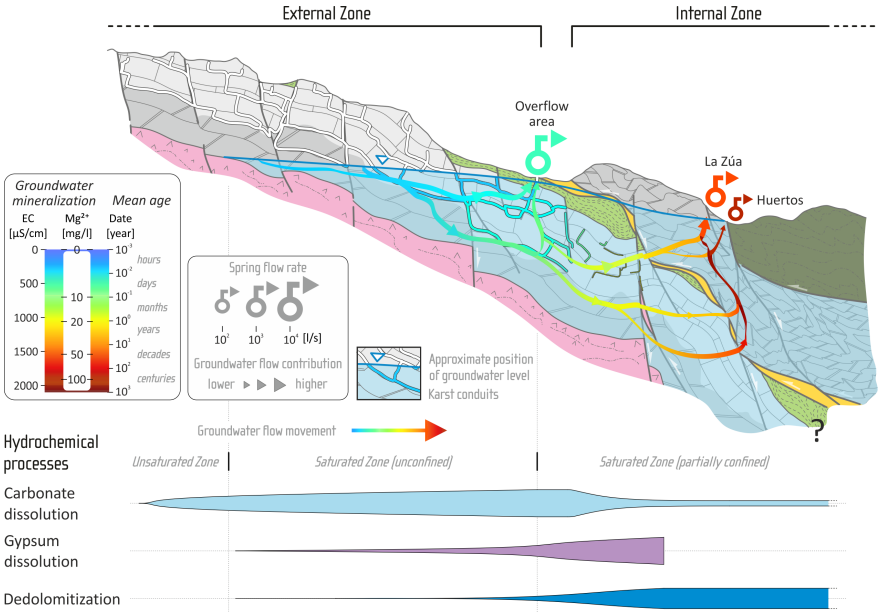

Hosted file

Table_1.docx available at https://authorea.com/users/305548/articles/436280-complimentary-use-of-dating-and-hydrochemical-tools-to-assess-mixing-processes-involving-centenarian-groundwater-in-a-geologically-complex-alpine-karst-aquifer

Hosted file

Table_2.docx available at https://authorea.com/users/305548/articles/436280-complimentary-use-of-dating-and-hydrochemical-tools-to-assess-mixing-processes-involving-centenarian-groundwater-in-a-geologically-complex-alpine-karst-aquifer

Hosted file

Table_3.docx available at https://authorea.com/users/305548/articles/436280-complimentary-use-of-dating-and-hydrochemical-tools-to-assess-mixing-processes-involving-centenarian-groundwater-in-a-geologically-complex-alpine-karst-aquifer

Hosted file

Table_4.docx available at https://authorea.com/users/305548/articles/436280-complimentary-use-of-dating-and-hydrochemical-tools-to-assess-mixing-processes-involving-centenarian-groundwater-in-a-geologically-complex-alpine-karst-aquifer